

CP40

SARin (and beyond) for Coastal Ocean

isardSAT Reference: ISARD_ESA_CP40_TN_320
Issue: 1.b

Prepared by: isardSAT CP40 team

12 October 2015
Activity: CryoSat+ for Ocean

This page has been intentionally left blank

Change Record

Date	Issue	Section	Page	Comment
9 July 2015	1.a	all	all	Initial Issue
12 October 2015	1.b	5.1, 5.2, 6	30, 36, 44-51, 55-56	Answers to ESA review

Control Document

Process	Name	Date
Written by:	Pablo García	12 October 2015
Checked by:	Mònica Roca	12 October 2015
Approved by:	Mònica Roca	12 October 2015

Distribution List

Company	Name
ESA	Jérôme Benveniste
SATOC	David Cotton
isardSAT	Pablo García Mònica Roca

Table of Contents

1	INTRODUCTION	5
1.1	SCOPE	5
1.2	ACRONYMS	5
1.3	REFERENCES	5
2	OVERVIEW	6
3	RESULTS FROM PHASE I.....	8
3.1	INPUT DATA SET	8
3.2	AREA OF INTEREST	8
3.3	ALGORITHMS	10
3.4	PHASE I RESULTS	12
4	PHASE II: SARIN	17
4.1	FIRST APPROACH	18
4.2	SECOND APPROACH.....	19
5	PHASE II: BEYOND SARIN.....	27
5.1	THIRD APPROACH	27
5.2	DELIVERED DATA.....	39
5.3	OPEN OCEAN RETRACKER ASSESSMENT	50
6	CONCLUSIONS.....	52

1 Introduction

1.1 Scope

The scope of this document is to describe the investigation carried out by the isardSAT team within the CP4O project Phase II. It is about improving the results of the first Phase of the project (AD 2) about a scientific study of the capability of CryoSat-2 Synthetic Aperture Radar interferometry (SARin) mode to mitigate the echoes contamination on coastal ocean areas. It also explains a standard processing for other modes (SAR and LRM) in order to improve the SSH retrievals in Coastal Ocean scenario.

1.2 Acronyms

AoA	Angle of Arrival
AoI	Area of Interest
CS2	CryoSat-2
CP4O	CryoSat Plus for Ocean
DS	Data Set
L2I	Level 2 Intermediate/Interim (ESA product)
LEP	Leading Edge Point
LRM	Low Resolution Mode
NOC	National Oceanography Centre
OSM	Open Street Map
S3	Sentinel-3
S6	Sentinel-6
SAR	Synthetic Aperture Radar
SARin	Synthetic Aperture Radar interferometry
SSH	Sea Surface Height
TBD	To be defined

1.3 References

- AD 1 CryoSat +: Ocean Theme. CP4O-Cryosat Plus 4 Oceans. Technical Proposal. November 2011. SATOC, DTU Space, isardSAT, NOC, Noveltis, STARLAB, TUDelft, University of Porto and CLS.
- AD 2 CP4O: SARin for Coastal Ocean. WP4000 ATBD Contribution, Technical Note, ISARD_ESA_CPO_SCO_ATBD_225, isardSAT December 2013.

2 Overview

The investigation developed in Phase I of this project was based in a uniqueness of the CryoSat-2 (CS2) mission: its capability to operate in Synthetic Aperture Radar interferometry (SARin) mode, thanks to carrying on-board a fully duplicated altimeter system for the processing of the echoes received by two antennas simultaneously.

This mode allows for deriving the angle of arrival (AoA) of the echoes in the same direction of the antennas baseline (across-track direction as shown in Figure 2-1). This capability adds to the SAR enhanced along-track spatial resolution (see central footprint on Figure 2-1), the ability to determine the origin of the echo across-track, specifically the angle of inclination from Nadir (see right hand side footprint on Figure 2-1).

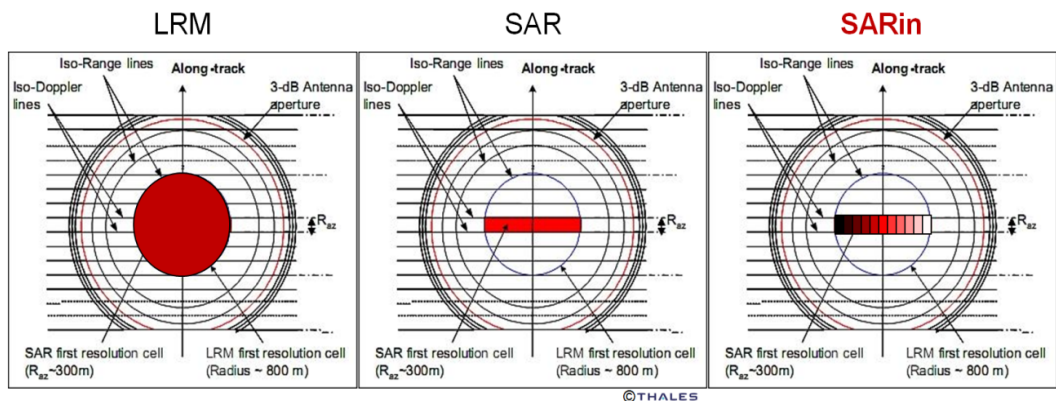


Figure 2-1. The three CS2 possible modes: LRM, SAR & SARin (courtesy of Thales Alenia Space).

The AoA is derived from the phase information of the signals received by the two antennas. For equal phase between echoes (zero difference between them), the backscatters are classified as Nadir. Otherwise, it shall be proved that the echo comes from one side or the other of the sub-satellite track in the across-track direction.

In Figure 2-2 we can observe, in a case of a coastal ocean scenario, the well-known power waveform on top of the figure, and the less known AoA waveform (intrinsic to the SARin mode) on the bottom. We can see how the two clear peaks of this contaminated power waveform are in line with two correspondent coherent (less noisy) AoA zones: the peak on the left, very specular, shows a AoA far from zero, the peak on the right, ocean like, is in line with the red line reference (AoA = 0) crossing.

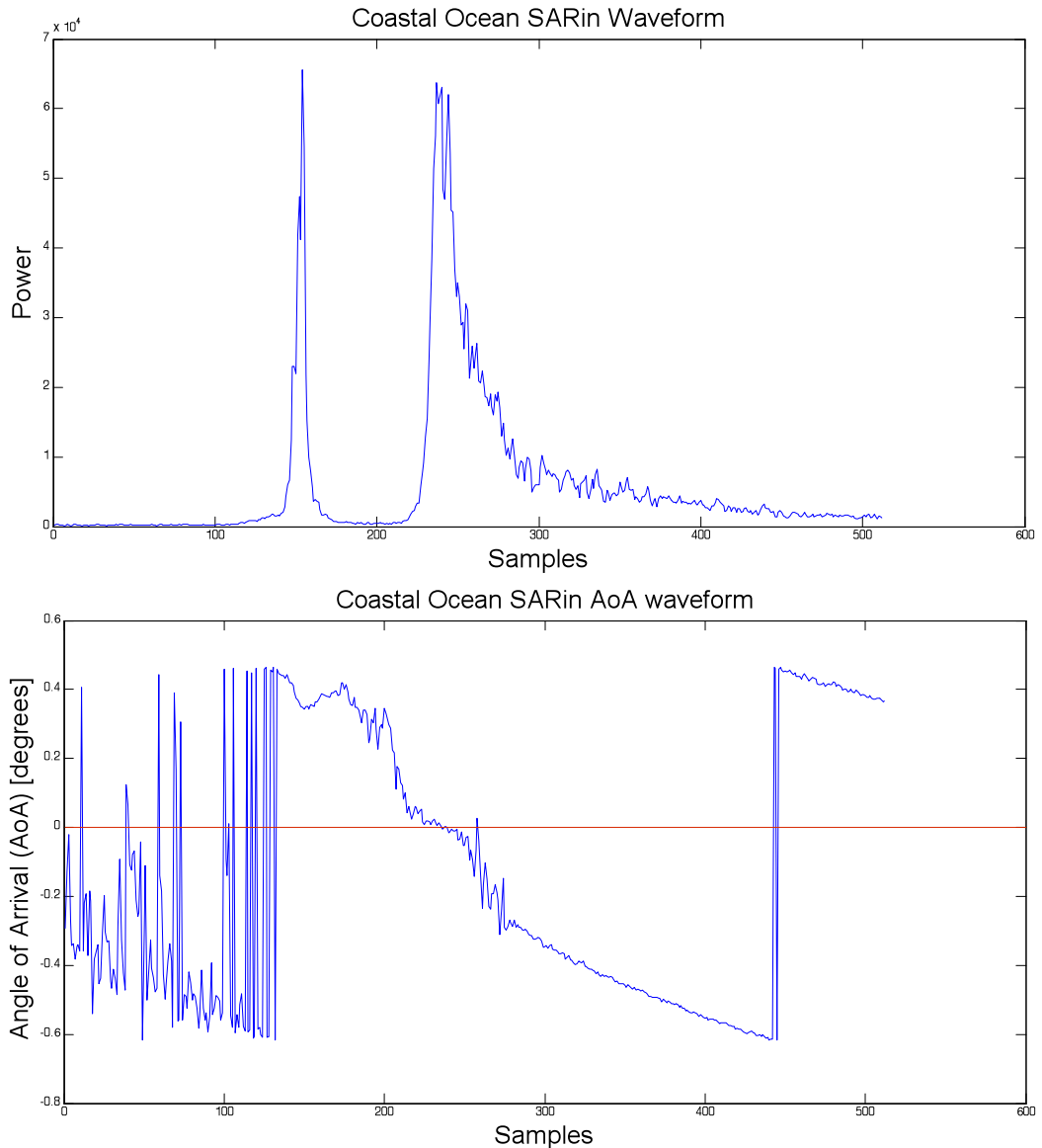


Figure 2-2. Example of a Coastal Ocean contaminated waveform. TOP: Power waveform. BOTTOM: Angle of Arrival waveform.

With this data in our hands, we can discriminate the specific Nadir ocean signal within the waveform.

Knowing that our interest is focused in the Sea Surface Height (SSH) estimates, and that a Nadir AoA (AoA = zero degrees) is what we expect to detect from the sub-satellite track ocean surface while approaching the coast, any AoA response far from zero can be considered in this study as a target to be avoided.

This is the general approach of the small scientific investigation within the CP40 project Phase I that has the aim of improving the sea surface topography estimation near the coast with CS2 SARin data (AD 1).

3 Results from Phase I

In this chapter we will explain the results of the work done in the first Phase of the project, as an introduction of the improvements developed in the second Phase.

3.1 Input Data Set

The different products to be used for the investigation were expected to show different scenarios in coastal zones:

- Two initial geometrical configurations were required: some of the passes with the sub-satellite track parallel to the coast, and some others perpendicular.
- Different coastal land scenarios (low lands or cliffs), and diverse coastal zones with cays, reefs and others that can provide us with specular waters close to the track.

We discarded those tracks showing stability in SSH estimation along the track. We requested access to the L2I (Level 2 Intermediate / Interim) products where additional information is available (e.g. retracked range bin). L1b products were essential for performing the work, with the three available waveforms that characterize the received echo in the SARin mode, and permit a sample by sample analysis not possible with L2 product outputs; they are the power waveforms, the phase difference (thus AoA) waveforms, and the coherence waveforms.

3.2 Area of interest

For the development of this study, a particular SARin mode area was requested: the Cuban Archipelago, between latitudes 19 and 24 North and longitudes 73 and 86 West (see Figure 3-1). It was approved by ESA and implemented on the 1st of October 2012, when the CS2 mode mask V3.4 was activated.

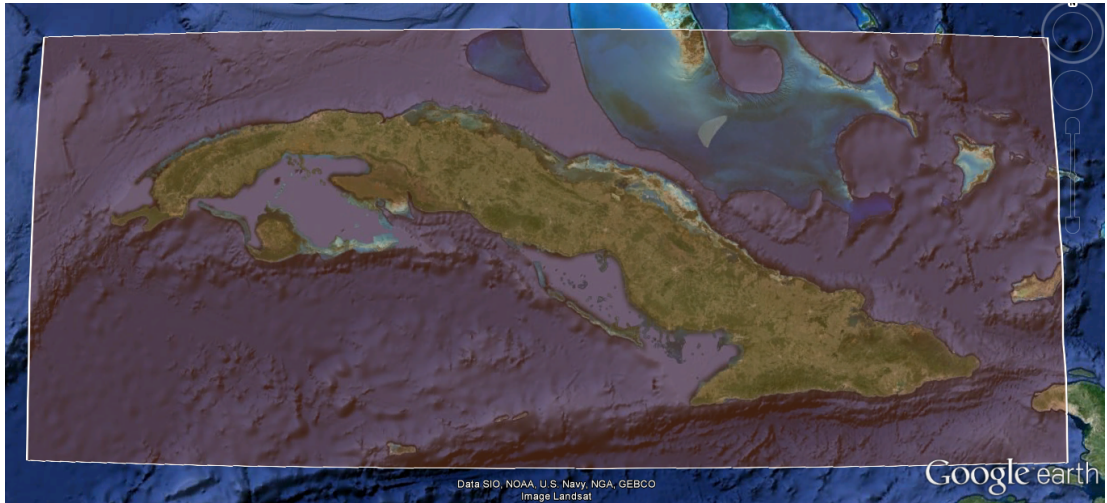


Figure 3-1. SARin patch covering the Cuban Archipelago.

The Cuban Archipelago is the most exploited zone for the study, but not the only SARin patch considered. In Chile, although almost the whole SARin patch covering the Andes has no coasts in it, there is a little part of it in the North near Peru around latitude 20°S that has proven to be interesting for the study, and also some tracks in the South near Chiloé around latitude 44°S (see Figure 3-2).

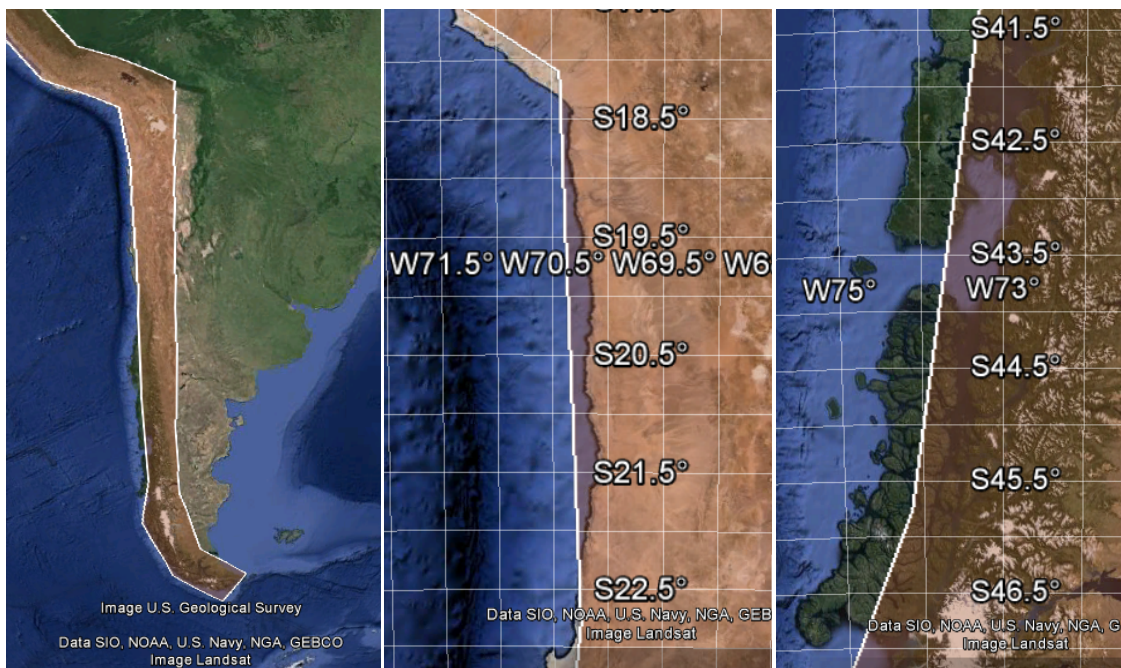


Figure 3-2. SARin patch covering the Chilean section of Los Andes (left), with coastal areas on the north (centre) and in the south (right).

Also SARin patches over some coastal zones of Norway, Iceland and Canada (see Figure 3-3) have been considered, but with the constraint of having the risk of sea ice situations, that could invalidate the study.



Figure 3-3. SARin additional zones over Norway (left), Iceland (centre) and Canada (right).

3.3 Algorithms

The whole investigation programming activities were developed in Matlab, from the ESA products reading routines up to the final results. The “L2 processing” tasks have been developed beyond the CP40 project, by isardSAT funding, with the aim of making possible a validation of the study results.

The data processing can be simplified into a two steps algorithm (see Figure 3-4). The L1b and L2I products are read and processed in a first stage, producing an input for the second stage that consists in a “seed” for the retracking. Then, the second step will retrack the waveforms coming from the L1b product, helped by the given seed. The L2I products are only used for the cross-comparison and validation of the final outputs.

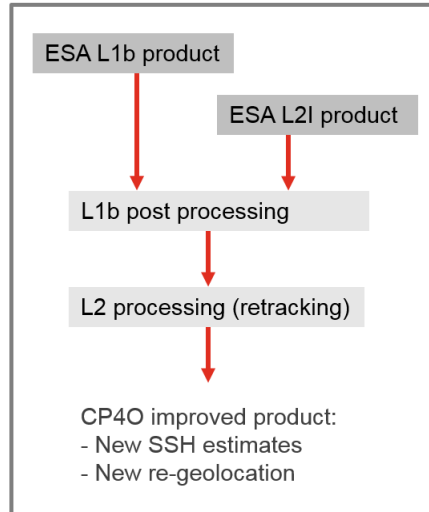


Figure 3-4. Simplified block diagram of the SARin investigation processing.

In Figure 3-5 it is showed a more detailed data flow of the algorithms that have been developed within the first stage of the processing, the “L1b post processing” block of Figure 3-4.

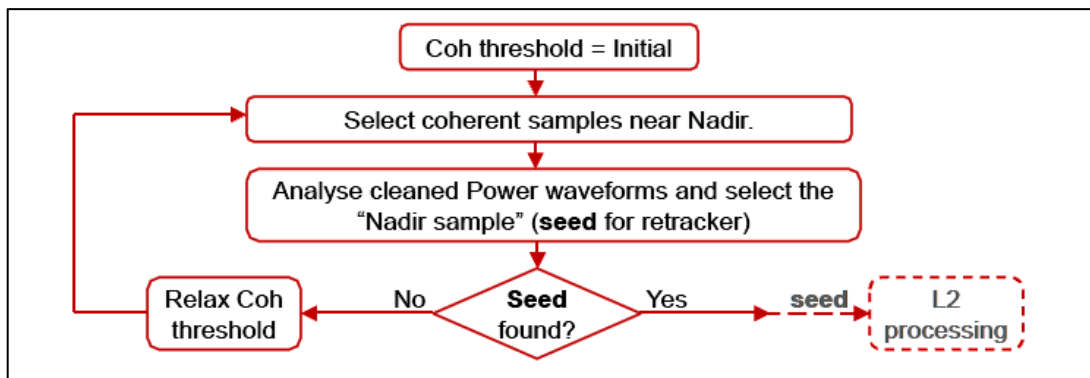


Figure 3-5. Block diagram showing the general algorithms logic of the L1b processing stage of the study.

The idea developed for the post-L1b processing stage is an iterative process that produces the final “seed” for each of the waveforms coming from the L1b product. See AD 2 for details.

3.4 Phase I results

Results are here shown as means of a set of figures following a standard configuration that consists in superimposing information on the map of a particular coastal zone of interest. The superimposed information will be the ESA (read from the L2I products) and the CP4O (our processing output) retracked geolocations, including SSH estimates over the track's section of interest. This representation seems to be the best manner to provide evidence of erroneous SSH estimates due to the non-proper focused retracking near the sub-satellite track (i.e. Nadir).

Here below, in Figure 3-6, Figure 3-7 and Figure 3-8 we show some examples of good results of the developed processing. In red, SSH as read from the ESA L2 products; note this show clear wrong estimates (in the form of jumps) when the track approaches the cays. This is well corrected by isardSAT processing strategy in CP4O; results are visible in yellow and show more stability than the previous all along the track. Also the retracked geolocations are corrected from the red points (ESA L2I) to the yellow points (CP4O isardSAT processing).

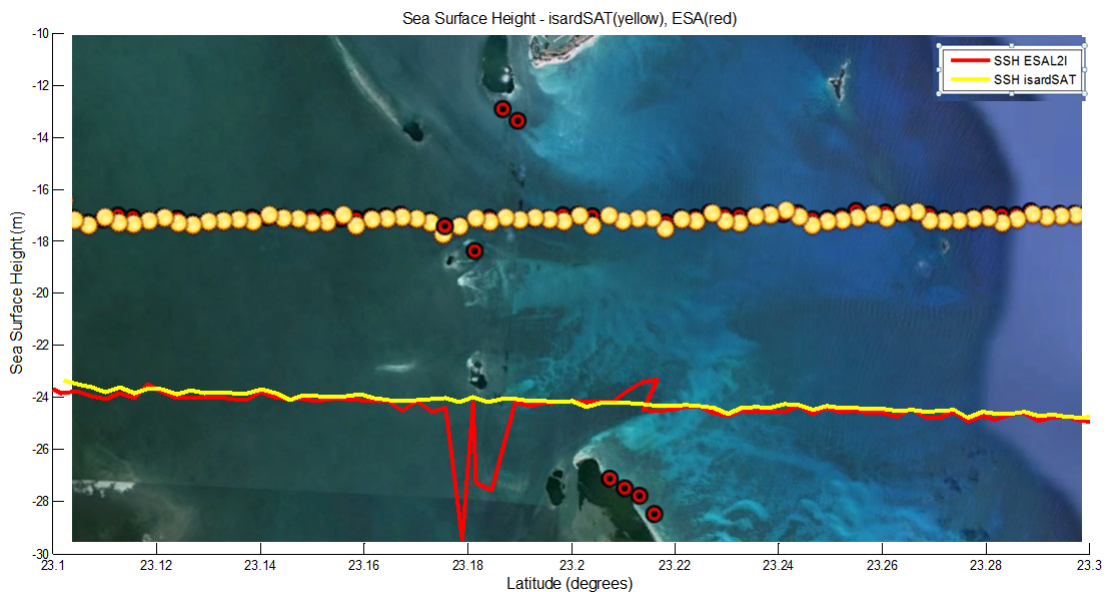


Figure 3-6. Example of processing results on Cuban North Cays near Varadero. Retracked geolocations are marked with points, and the SSH estimates (in meters) are marked with lines. Red colour is used for ESA L2 outputs, yellow colour is used for CP4O processing outputs.

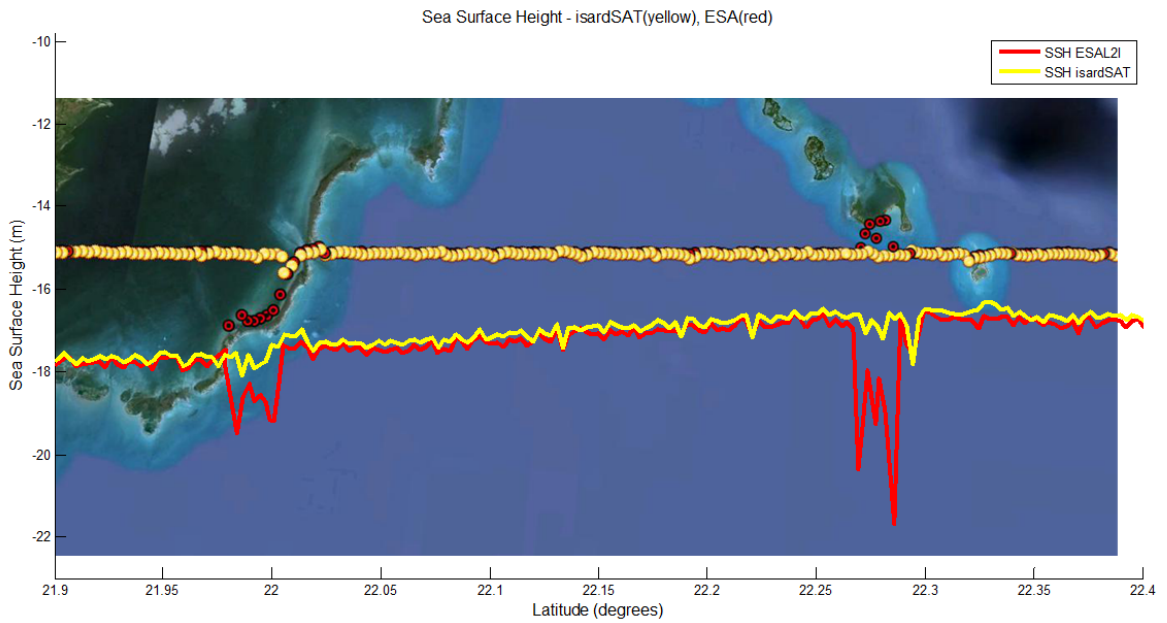


Figure 3-7. Example of processing results on Cuban South West Cays, ascending pass. Retracked geolocations are marked with points, and the SSH estimates (in meters) are marked with lines. Red colour is used for ESA L2 outputs, yellow colour is used for CP40 processing outputs.

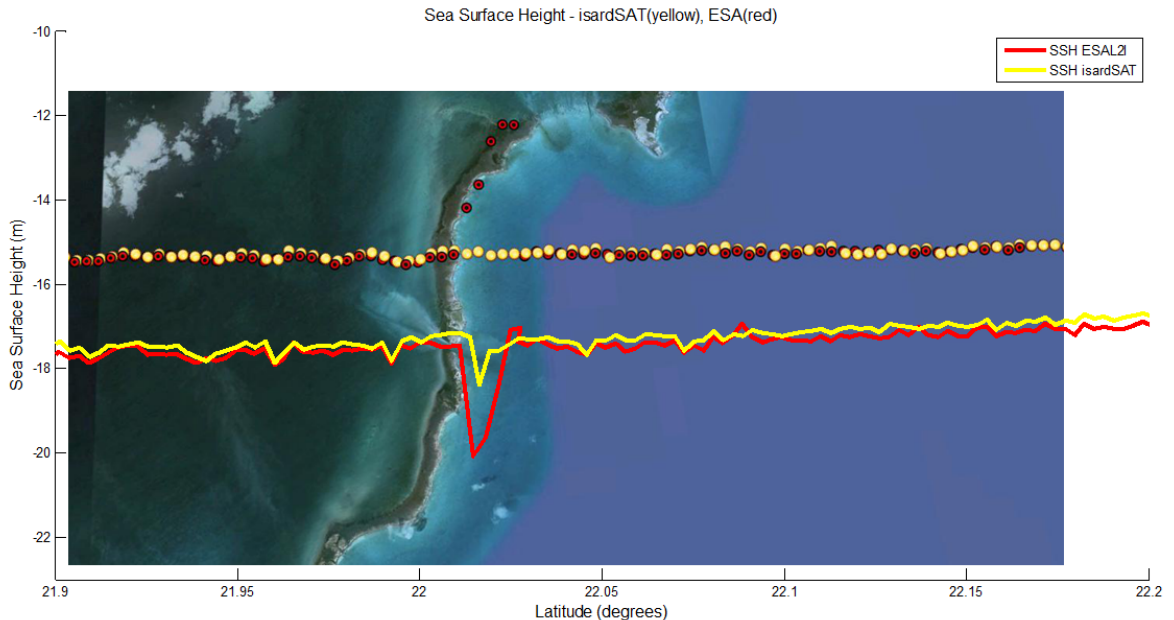


Figure 3-8. Example of processing results on Cuban South West Cays, descending pass. Retracted geolocations are marked with points, and the SSH estimates (in meters) are marked with lines. Red colour is used for ESA L2 outputs, yellow colour is used for CP40 processing outputs.

Although the solution proposed by isardSAT in CP40 has shown promising results, this is not always the case and hereafter we provide some evidence of false alarms (see Figure 3-9 to Figure 3-12).

Figure 3-9 shows a peculiar case in which although overall good performance along the track, there is a clear error; with a wrong geolocation in line with other ESA results, near the shore of one of the little islands in latitude 22.62°N, probably corresponding to a specular waters target. This record corresponds to the central waveform in Figure 3-10, where we can observe how the retracker is fitting (red line) the different waveforms. The retracted sample in the records before and after is the one corresponding to the Nadir SSH (the peak on the left side of the waveform) but then, in the affected SSH record, the retracker fitted the leading edge of the peak on the right side of the waveform, even though the seed given is around the Nadir range bins (on the left). The AoA of the peaks on the right side are far from zero, and the seed for the retracker was always indicating correctly the peak on the left side, but the retracker was unable in this case to follow the seed indications and avoid the wrong target. This is one of the cases to be solved in this Phase II of the project.

The second example, different from the previous but also interesting, shows the analysis of a parallel track to the coast-line on the Chilean North coast. This scenario includes cliffs and an airport relatively near the shore (see Figure 3-11). We observe how the geolocations far from Nadir are coincident with very specular airstrips surface locations.

Three records were corrected from five ESA L2 SSH errors. In Figure 3-12 we can see three consecutive waveforms fittings including the two CP40 algorithms bad SSH retrievals. In the three we can check the two clear peaks corresponding to the airport runway (lower range bin, specular surface echo shape) and to the sea surface (higher range bin, ocean echo shape). The waveform on the left is working as expected retracking the sea surface, while the other two waveforms on the

middle and on the right are retracking the airstrip targets that are presenting a more powerful echo than the one coming from the sea in Nadir. This case also is to be reprocessed and improved at Phase II.

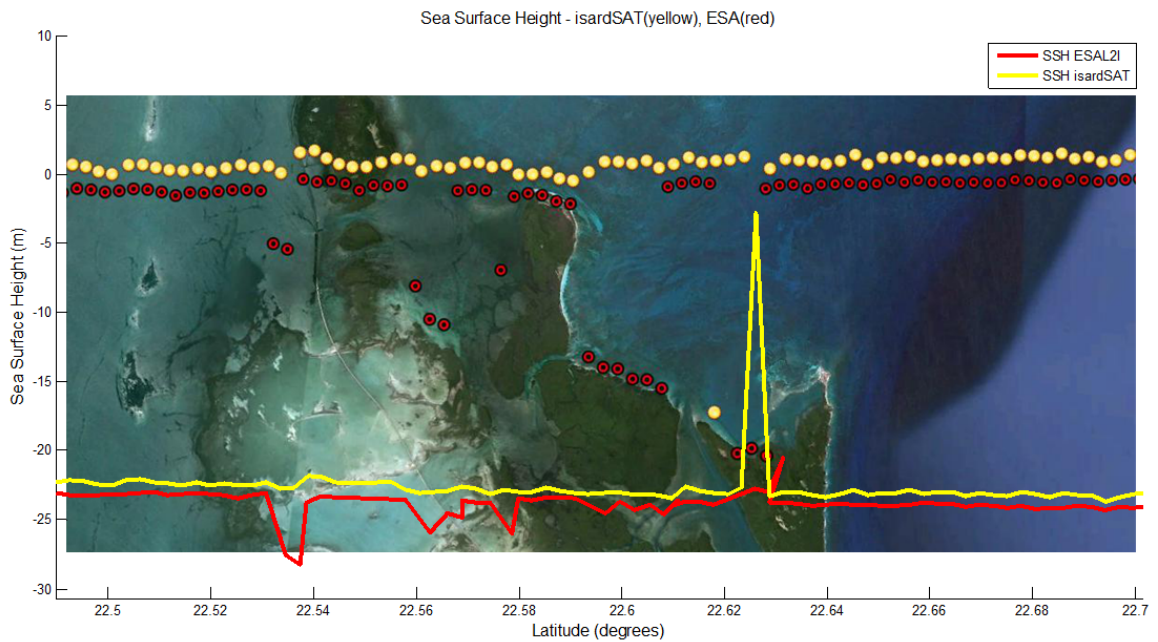


Figure 3-9. Example of processing results on Cuban North East Islands, descending pass. Retracked geolocations are marked with points, and the SSH estimates (in meters) are marked with lines. Red colour is used for ESA L2 outputs, yellow colour is used for CP40 processing outputs.

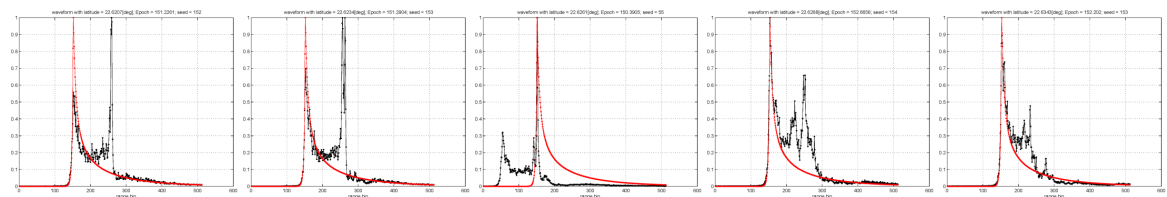


Figure 3-10. Five consecutive Power Waveforms corresponding to the track of Figure 3-9 around the CP40 processing SSH jump. The retracking fitted waveform is shown in red.

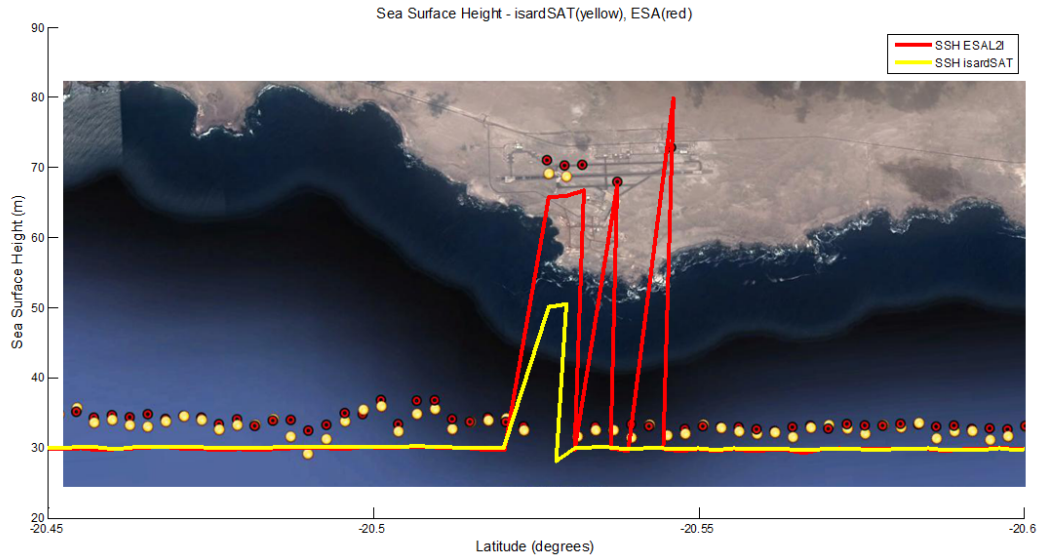


Figure 3-11. Example of processing results on the North Chilean coast. Retracked geolocations are marked with points, and the SSH estimates (in meters) are marked with lines. Red colour is used for ESA L2 outputs, yellow colour is used for CP40 processing outputs.

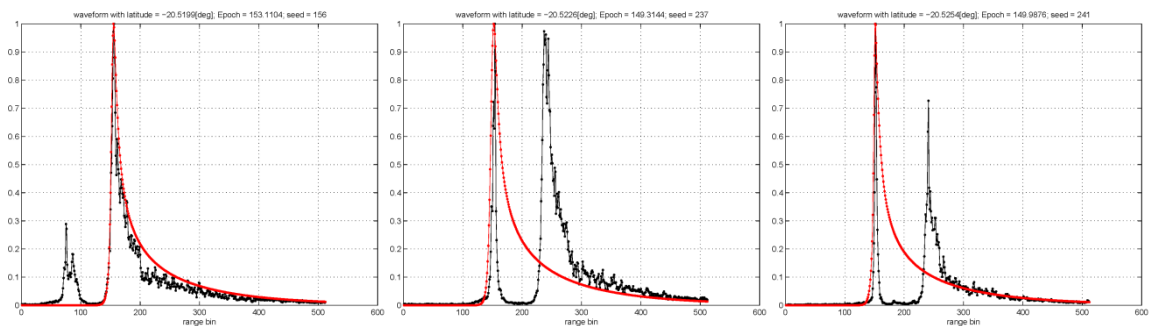


Figure 3-12. Three consecutive Power Waveforms corresponding to the track of Figure 3-11 around the first CP40 processing SSH jumps on the left side. The retracking fitted waveform is shown in red.

The cases of tracks perpendicular to the coast are not showed because, as expected, they are not presenting so much signal degradation. Also the scenario of inland waters have been addressed, but it is not showed here because the ESA L2 SSH results were already good. It is the case of Titicaca Lake, in Andes.

Finally, there are cases with no solution. This is usually happening with waveforms with a too high level of contamination, or presenting a power peak very close to the ocean surface leading edge. It is something to be addressed in the second phase of the project. Anyhow there is a limit we cannot cross in terms of retrieving sea surface information from waveforms presenting a high level of degradation.

4 Phase II: SARin

The main purpose of the second phase of the study is to develop and apply improvements on the sea level retrievals in coastal zones echoes using the CS-2 SARin mode products, starting from the phase I achievements.

Some cases, as the two showed from Figure 3-9 to Figure 3-12, presented improved SSH series, but with some records with errors, both in the retracked geolocations and the SSH estimates. The reason why it is happening is related to the second part of the processing: the retracking algorithm. The seed inputted from the post-L1b processing is correct, indicating the Nadir range bin, but the retracker fitting routine neglects it and iterates until the highest power peak is retracked.

The improvements were initially thought to be developed in the first of the two main chains of the algorithms: the post-L1b processing. But due to the level of link between the two processing stages, it was also necessary to develop some changes in the second stage: the retracker. The differences between both approaches are explained in 4.1 and 4.2.

The AoI set for this study is represented in Figure 4-1 (green sub-box).

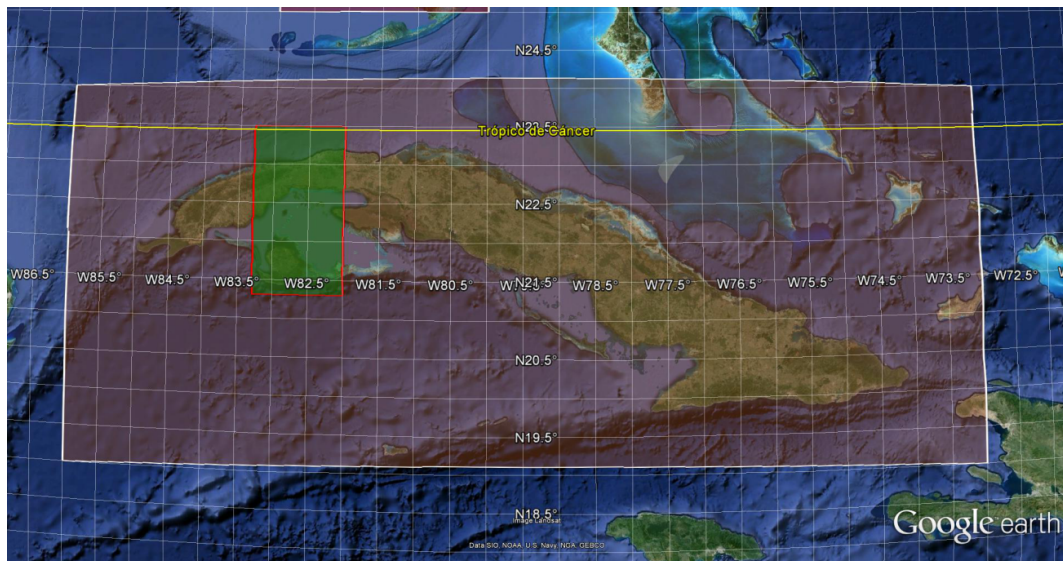


Figure 4-1. Area of Interest of the study developed in this second phase of the CP40 project (green sub-box inside the general SARin geographical area covering Cuba).

In Figure 4-2 we can see the 104 tracks downloaded for this study, from October 2012 to the end of 2014.

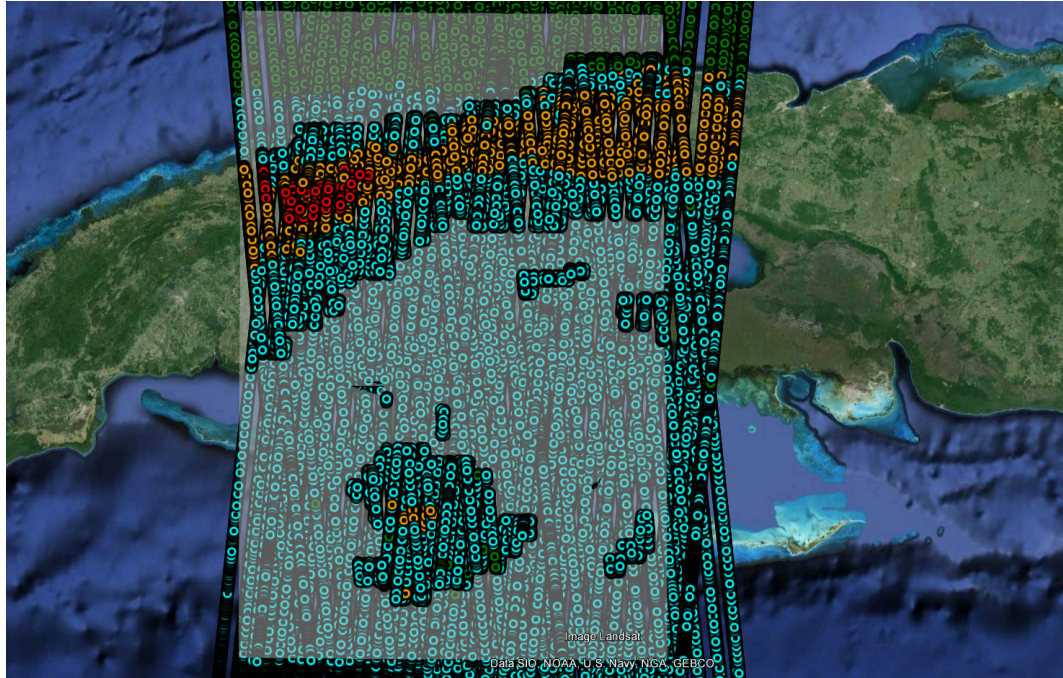


Figure 4-2. Tracks corresponding to the 104 products used for the study.

4.1 First Approach

The situation of Figure 3-12 (central plot) is identified as a clear issue that can be managed in further improvements of the post-L1b algorithm. The visible detaching between the two targets signals in the range window indicates that there is space for a possible solution. The example of Figure 3-10 can be addressed in the same way, but here the ocean waveform trailing edge is not clean but distorted by another backscatter contribution.

The limitations of the above Phase I solution can be solved with an additional work on the available AoA and power waveforms after the third step of the post L1b processing. The coherence waveform is also used in the previous post_L1b processing step, dynamically set from 800 to 200 depending on the level of coherence of the near Nadir samples.

The main idea is to avoid the contaminated sections in the waveforms and interpolate the samples in those gaps. The AoA data will help us in determining the waveform range bins far from Nadir (set as more than 0.07° of AoA). The power waveforms will indicate, within the far from Nadir range bins, the waveform section to be de-contaminated (power set as over $0.25 \cdot \text{maximum waveform power}$). All the range bins above the thresholds will be substituted by an interpolation between its section extremes.

With this approach we can clearly solve the case of Figure 3-12. The second Phase I fail case of Figure 3-10 could be also solved, but the trailing edge of the waveform will be affected. Some other cases of coastal echoes with a higher level of contamination are more difficult to solve. Several sections of the echo could be affected by the coastal contamination, and after the current proposed method, the waveform could remain being too much degraded, and the SSH retrieval invalidated.

The number of these unsolved cases due to the degradation of the coastal waveforms after applying the proposed approach ended up being not negligible, and the solution to tune such a processing too complicated. An alternative was needed.

4.2 Second Approach

The alternative to the above approach was not based in changing the waveform shape, but selecting a waveform section to be interpolated. For this approach was necessary to adapt the retracker routine in order to process a dynamic waveform section around the seed.

The solution consists in cutting the waveform around the seed (output of the first processing stage). The number of range bins to be cut was carefully assessed trying with a significant number of cases and checking the retracker performance. Finally it was decided to cut 25 range bins before the seed (enough to start the retracking from the thermal noise level) and 10 range bins after the seed (enough to get sufficient information from the trailing edge but not to much so the potential contamination remains outside the cut waveform section).

The retracker was tuned to dynamically retrack only the selected section of each waveform in the track.

For avoiding some possible additional peaks in the trailing edge, the waveform range bins with higher power than the seed at the right side of the seed range bin position were flattened. It must be noted that the seed is selected as the highest power range bin of all samples near Nadir (see AD 2). Near Nadir here means an AoA below 0.035° , hence an across-track distance of around 450m. Initially it was considered the same approach for the samples at the left side of the seed, but the retracking solution was highly degraded, therefore this option was discarded.

Here below we can take a look at some mesh plots of the SSH results of the ESA L2 products (Figure 4-3 for 2013 and Figure 4-5 for 2014) and CP4O second approach (Figure 4-4 for 2013 and Figure 4-6 for 2014).

The CP4O output is improving the ESA L2 results, showing a better read of the surfaces in both land and ocean surfaces. We can observe better in Figure 4-4 (CP4O output 2013) than in Figure 4-3 (ESA L2 2013) the elevations of "Isla de Pinos" in the South part of the mesh, and the beginning of the Cuban mountain system of "Sierra del Rosario" in the North-West part of the big island.

Specially the coastal zones are notably improved, avoiding the noisy ESA L2 SSH results. Nevertheless, in Figure 4-7 we can see some detected undesired outputs from our CP4O processing.

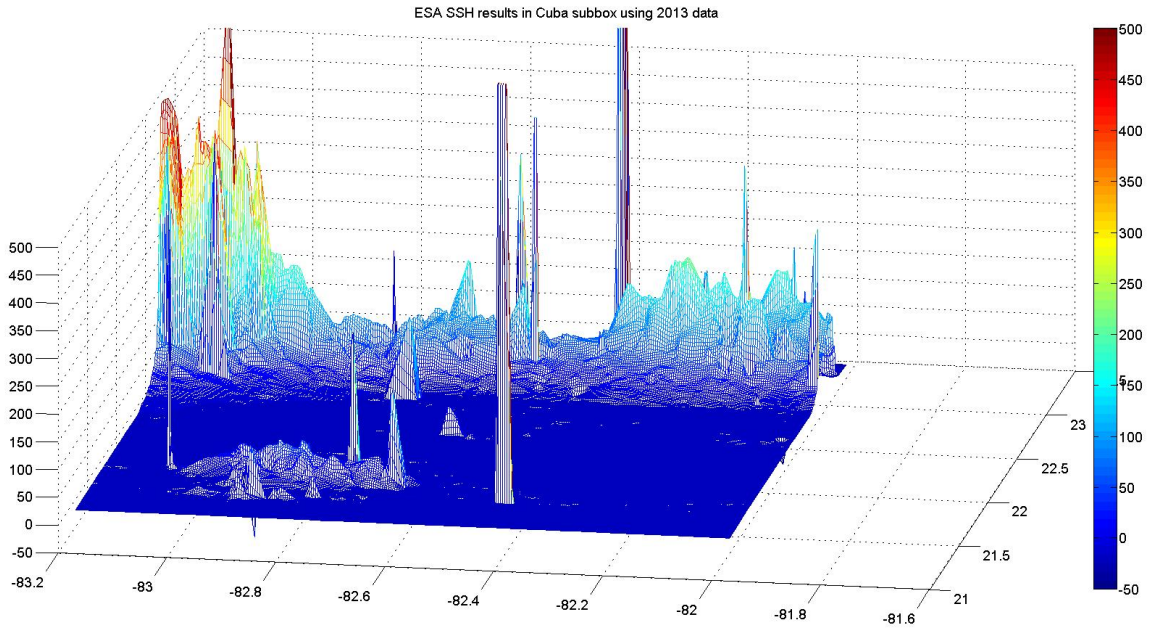


Figure 4-3. Mesh showing the ESA L2 products SSH results in 2013. Longitude in X-axis, Latitude in Y-axis, SSH in Z-axis.

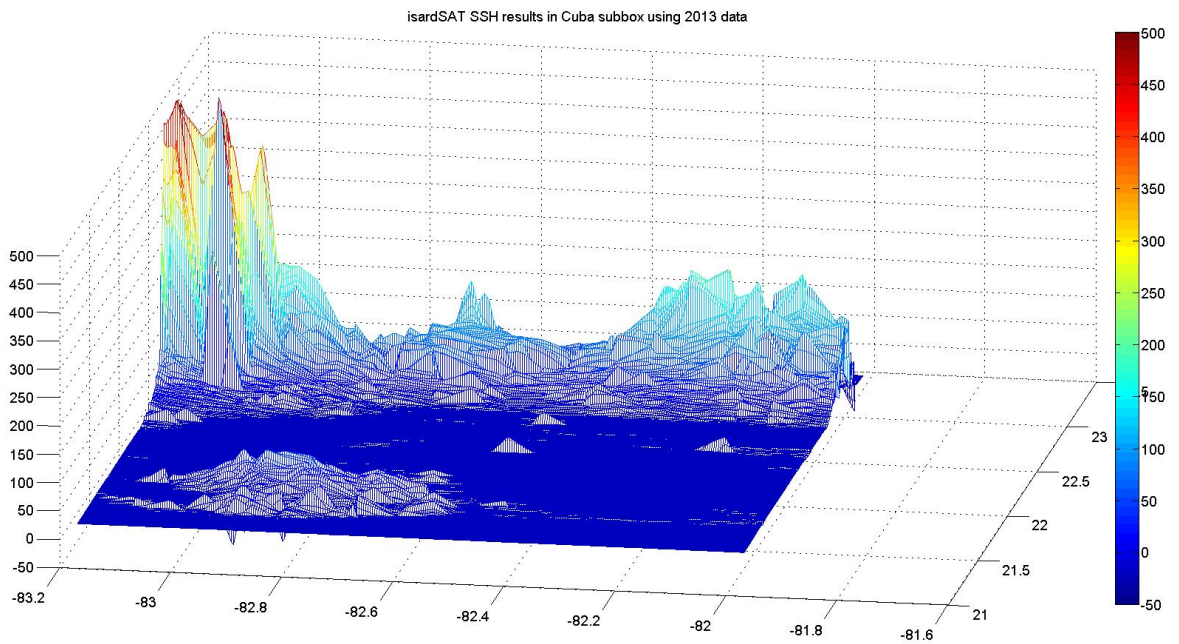


Figure 4-4. Mesh showing the CP40 SSH results in 2013. Longitude in X-axis, Latitude in Y-axis, SSH in Z-axis.

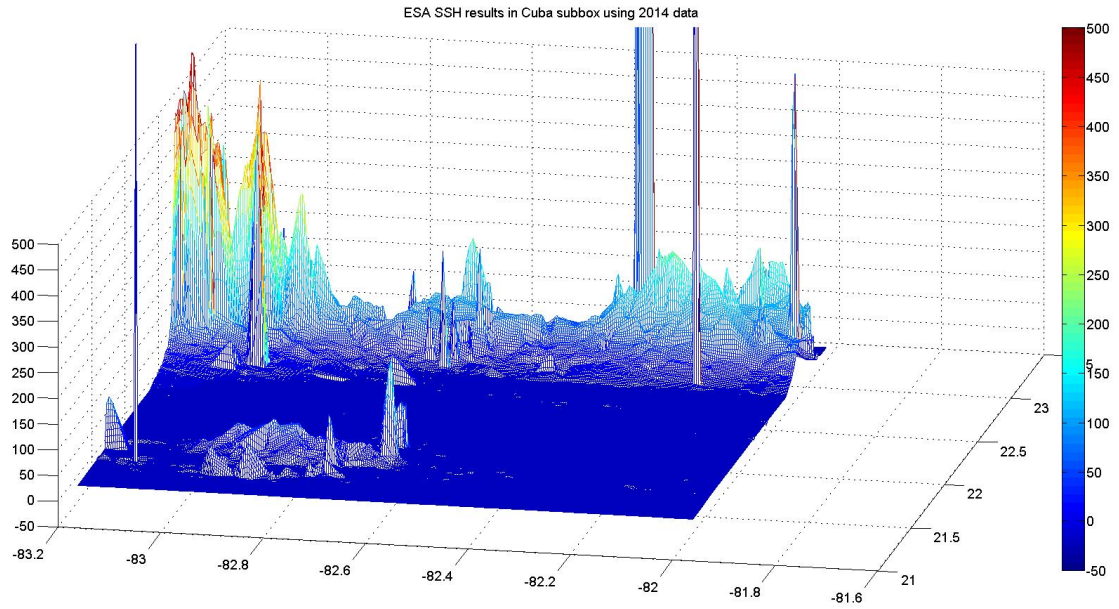


Figure 4-5. Mesh showing the ESA L2 products SSH results in 2014. Longitude in X-axis, Latitude in Y-axis, SSH in Z-axis.

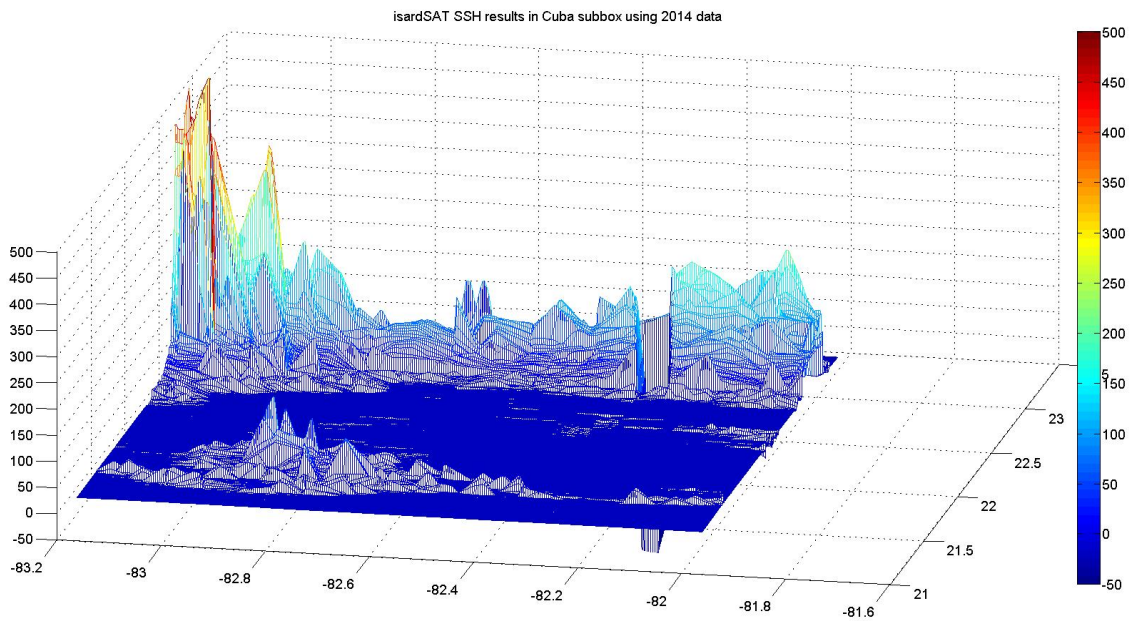


Figure 4-6. Mesh showing the CP40 SSH results in 2014. Longitude in X-axis, Latitude in Y-axis, SSH in Z-axis.

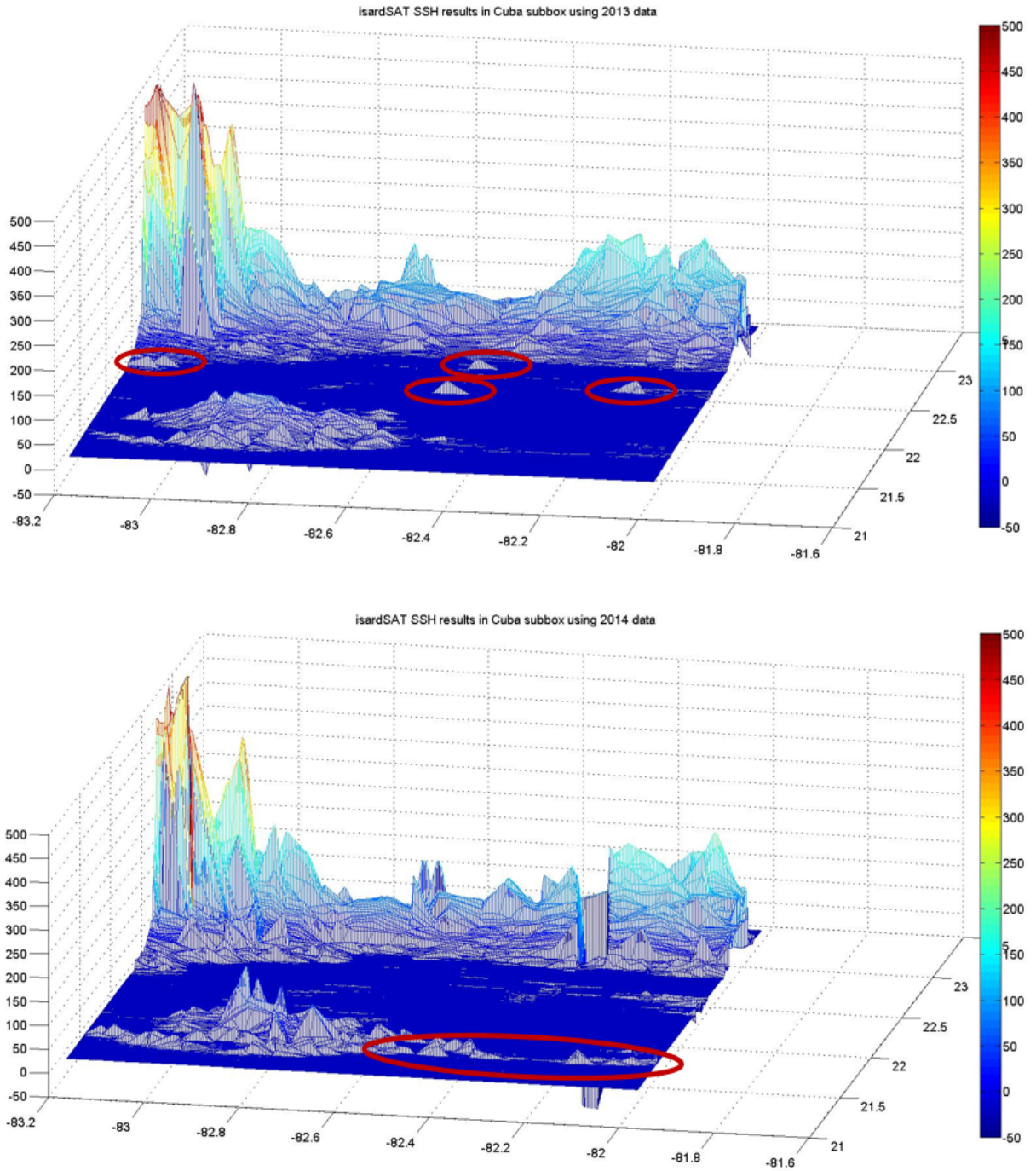


Figure 4-7. Some undesired Coastal Ocean SSH retrievals from the CP40 study. Longitude in X-axis, Latitude in Y-axis, SSH in Z-axis.

Several cases of wrong SSH results of the first approach were solved with this second approach. But there was an additional (not expected) observation that invalidated also this approach, and any other that could be based in the Phase Difference information to select the targets near Nadir.

In Figure 4-8 we observe an Open Ocean waveform, where it is showed both Power and AoA waveform. It is evident that the near LEP waveform section coincide with the one near Nadir: the AoA is very close to zero. The across-trak distance computed from the tagged sample AoA (0.0025°) is around 30 meters, very close to the sub-satellite track.

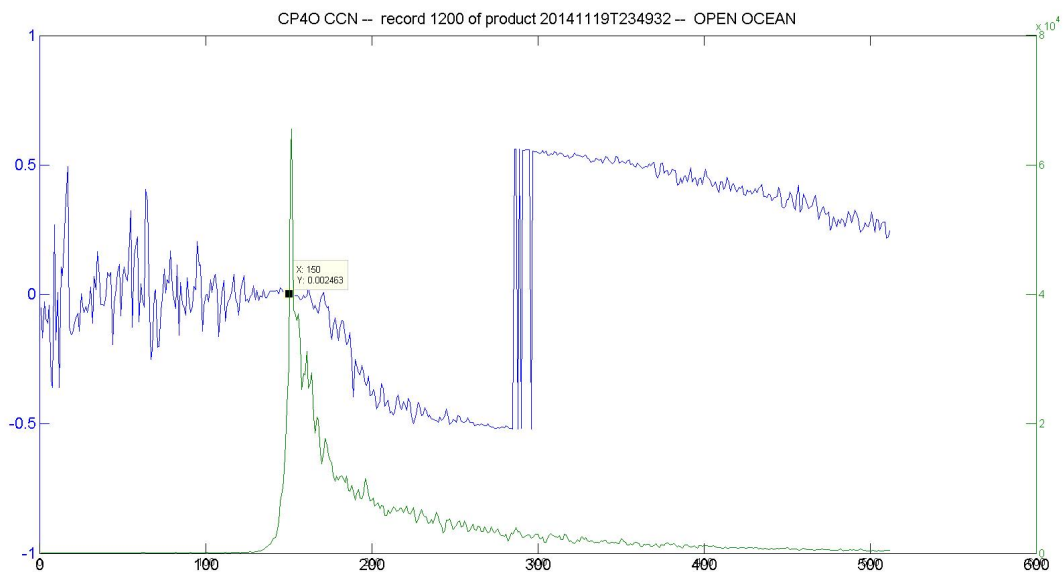


Figure 4-8. Open Ocean waveform in product of date 2014/11/19, time 23:49:32. Power (green) and AoA (blue) waveforms.

The tracks over the ocean passing close to the coastline should have at least a section in the waveform with AoA values close to zero. There are some cases of too much contaminated echoes were it is not possible to retrieve the Nadir waveform section, but it should not happen in an extended series of records in a track. Although it is not expected, this is what we have observed in the case showed in the below figures.

In Figure 4-9 we can see a coastal waveform with no AoA close to zero, although the power waveform shows a quite specular ocean waveform, as it is usual to happen in coastal scenarios as reefs and cays. The waveform does not present a high level of contamination, at least in the leading edge. The LEP range bins shows AoA with values far from Nadir, around 800m off-Nadir. No other section of the waveform have stabilised AoA values close to zero. A similar situation is showed in Figure 4-10, with closest range bins to Nadir around 500m off-Nadir.

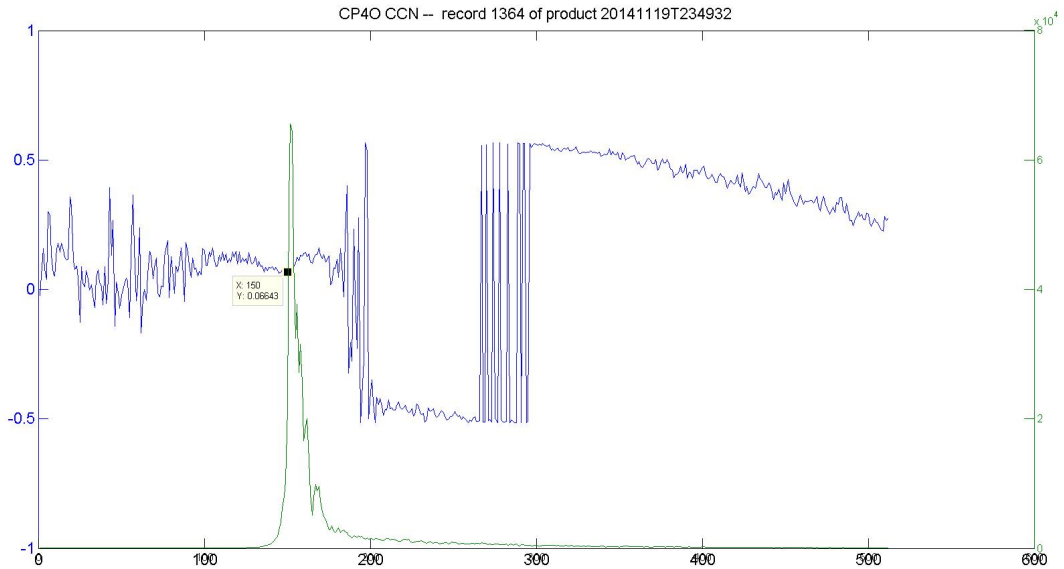


Figure 4-9. Coastal Ocean waveform in product of date 2014/11/19, time 23:49:32. Record 1364. Power (green) and AoA (blue) waveforms.

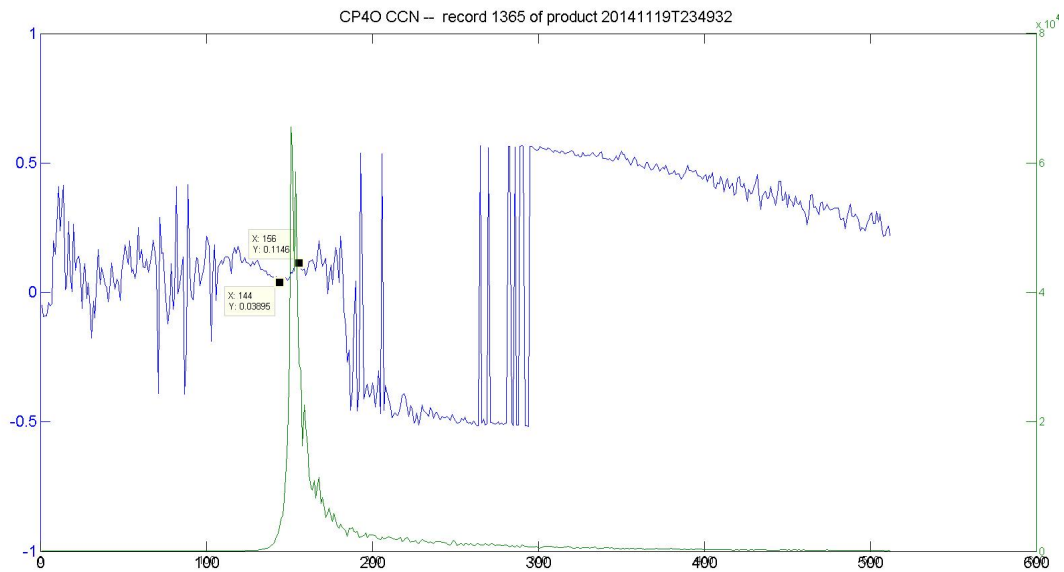


Figure 4-10. Coastal Ocean waveform in product of date 2014/11/19, time 23:49:32. Record 1365. Power (green) and AoA (blue) waveforms.

The coastal scenario where this track section is located is shown in Figure 4-11. A series of cays are close to the subsatellite track, being the closest position around 700m. The record 1364 tagged is the same of Figure 4-9.



Figure 4-11. Coastal scenario, section analysed with no AoA near Nadir.

If we take a look at Figure 4-12 we can see the sub-satellite track superimposed in a plot of the across-track distance waveforms (computed from the Phase Difference waveforms). The record 1364 observed in Figure 4-9 is also tagged here, highlighted with the red arrow. It is clear that when the track is travelling close to the cays on its right side, the Phase Difference waveforms are affected. The across-track distance of both tagged records range bins are detailed in the graph. The upper Open Ocean record range bin is close to 60 meters, while the Coastal Ocean record 1364 range bin is around 800m. It is visible how the across-track distance values are not close to zero around record 1364 in any clear stabilised waveform section, in an extended section of the track around 25 records (7500m along-track).

A possible interpretation of this situation is an across track surface slope, but here the waters are constantly shallow in a wide area, and the geoid is not presenting the changes that the plot shows between the affected coastal zone and the adjacents. Moreover, the expected stabilized AoA area is not seen around any other AoA value, neither far from Nadir.

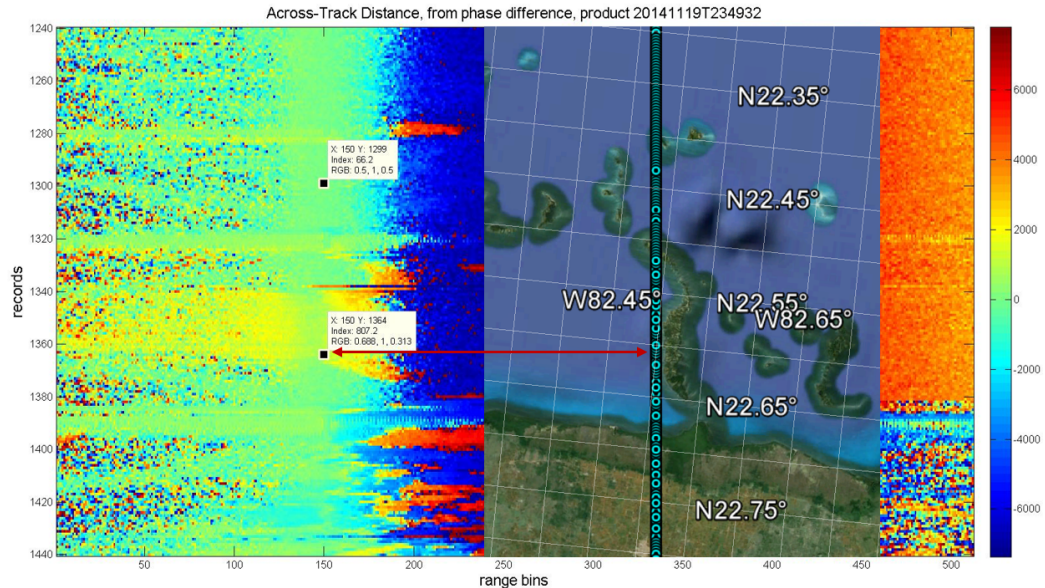


Figure 4-12. Google Earth image superimposed in the across-track distance plot around the track section with no coastal records range bins near Nadir.

The impact of such a coastal records AoA behaviour is very high in our coastal waveforms processing. The seed production is invalidated in these cases. The selection of the seed is based, among other restrictions, in a AoA tolerance that is here overcome.

The waveform section selection to be retracked depends totally on the seed reference.

If this happens in isolated records, it could be permitted. But it cannot be permitted for a continuous section of more than 20 records. The solution output quality could be too much degraded.

Once more, it is needed an additional approach. And now the Phase Difference is not a candidate to be taken into account for the retracking seed production, due to the above described problems. It is necessary a complete change of approach.

The new solution is described in the following chapter.

5 Phase II: beyond SARin

The different solutions adopted so far in the CP4O isardSAT tasks have had in common the use of the Phase Difference to distinguish the Nadir ocean target from other targets in order to retrieve better estimates of SSH after retracking. The Phase Difference data is intrinsic to a unique operational mode in the altimetry missions up to date: the SARin mode. So far no other altimeter has performed or planned measurements in this mode. Therefore, all the above solutions are only valid for this mode of the CS2 mission.

Fortunately, the problems found in the previous approach has led us to a significant step forward: to develop a solution that is suitable for all satellite modes (including SARin). If this works, it could be exploited for previous missions such as EnviSat, Jason 1 / 2, for future missions like S3 or S6, and for other CS-2 modes.

5.1 Third Approach

For the third approach we take advantage of a significant part of the algorithms developed in the previous SARin approaches, so the work has not been in vain.

It must be noted that the current configuration of the coastal processing is set from the coast up to 5 Km offshore for all the three approaches.

The variable that has been selected for this new approach is the Window Delay (i.e. Tracker Range). The variations over the ocean that can suffer this parameter along a track are expected to be smooth. If a sudden jump is observed in the Window Delay over the ocean, it is certainly due to the presence of a target that does not correspond to the Nadir Ocean surface. If we know the magnitude of the Window Delay jump, we can determine how far within the tracker window has gone the real Nadir Ocean target, and correct the jump accordingly. Therefore, it could be possible to follow the Nadir Ocean target along an ocean track, up to the coastline, as long as the tracker window has enough information about that target (i.e. the Window Delay jump does not causes the ocean signal to fall outside the tracking window). Again, as in the Second Approach, the waveform will be cut around the seed, but now the seed is produced by correcting the Window Delay variations.

The first idea was to check the Window Delay deltas between records, but this is sometimes hard to solve when the window delay shows a noisy behaviour. Hence, the solution adopted was to smooth the Window Delay series along the track and consider the smoothed series as the reference to be compared with the Window Delay. The differences between the Window Delay and the smoothed Window Delay are used for the seed production.

Also the track sections over the sea surface have to be identified in order to fit only the Window Delay series over the ocean, and do not incorporate information from land where the tracker starts to follow the land surface and could distort the tracker fitting output. A special emphasis has been done in this task. Initially the GSHHS land sea mask was used to set the limits between the track sections over the sea, but it was not reproducing with enough quality the Aol scenario. Then, thanks to the kind help of Paolo Cipollini (NOC), we were able to exploit the Coastal Proximity parameter data, being a much more suitable model for this application. However, again the data was not following all the details of the complex topography. Finally, the proper mask applied for the ocean sections determination was derived from the Open Street Map (OSM), showing an outstanding agreement

with the Google Earth images, with errors more than one order of magnitude below the previous masks.

Hence, using the OSM land sea mask, the distance of each record with respect to the closest land polygon was computed, and the ocean sections of each track were derived. Now we know the sections where the Window Delay will be smoothed. In order to have realistic smoothing computations, the land or ocean sections of less than 10 records were discarded and attached to the adjacent sections.

For the Window Delay smoothing, an initial solution applying a polynomial fitting was adopted. In Figure 5-1 we can see a CS2 track Window Delay series and two options of polynomial fitting with different degrees, 5 and 8. These two degrees were chosen only to demonstrate how much the results can vary if different polynomial fitting degrees are applied.

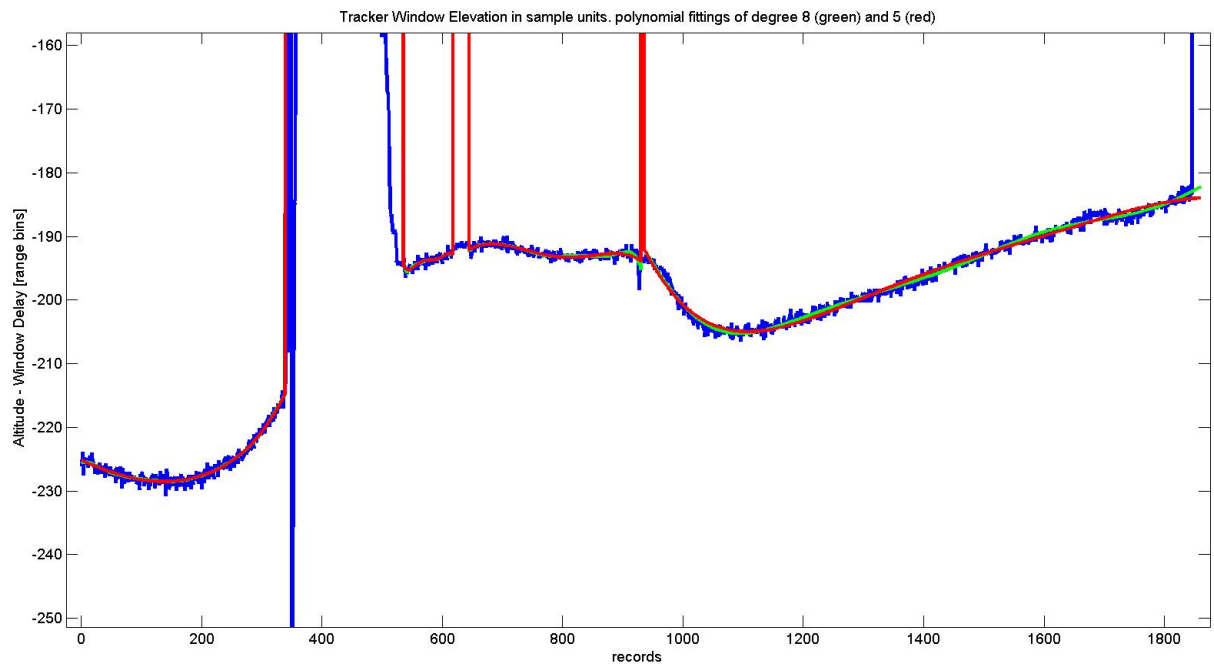


Figure 5-1. Window Delay (in range bins units, blue line) along a real track, from the 2013 CS2 L1b products database. Fittings of order 5 (red) and 8 (green).

After analysing the results of the residuals after the fittings, it was clear that the polynomial fitting degree was needed to be dynamical. Shorter sections need lower polynomial degree fittings, not to interpret Window delay noise as real signal. Longer sections, potentially showing more Window Delay oscillations, need to be fitted with higher polynomial orders.

The result of this specific algorithm step is depicted in Figure 5-2. If the third section was fitted with a high polynomial order, the results would be too much oscillating, following the Window Delay jumps.

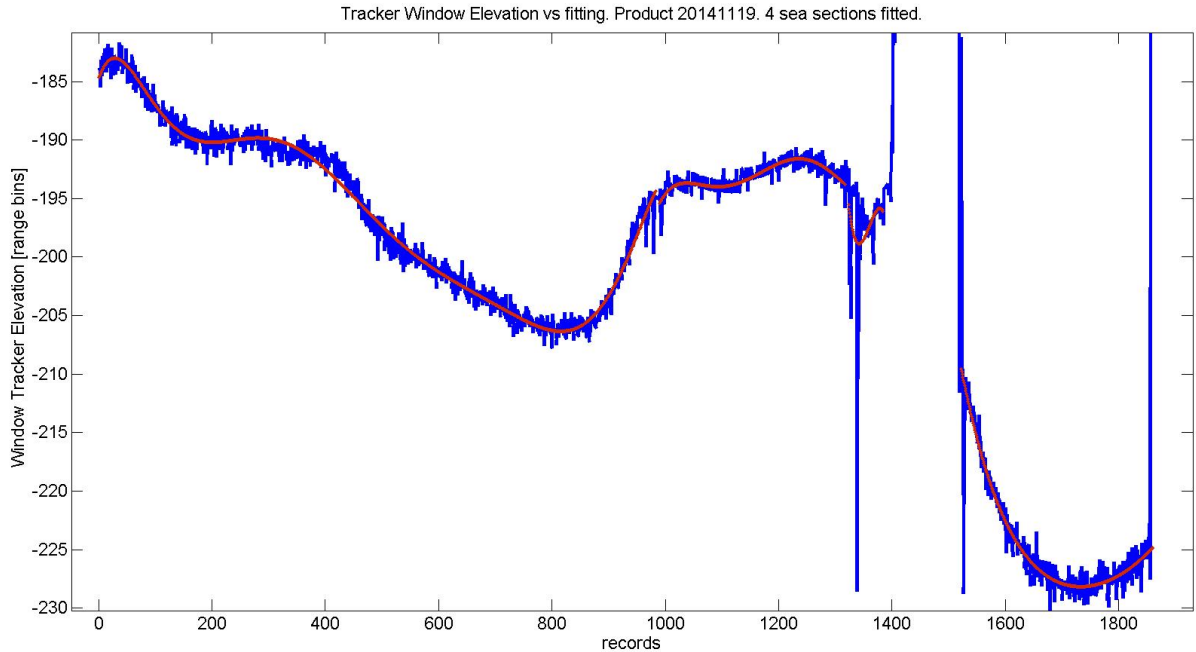


Figure 5-2. Window Delay fitting along the track of date 2014/11/19. Four different sections were fitted with different polynomial orders. In blue the original Window Delay, in red the fitting result.

After the smoothing, the seed is found taking into account the differences between the blue line (real Window Delay data) and the red line (the fitting result). Then, the retraking is done around the seed position.

A weakness of the above processing is the possible Window Delay data series detachment from the Ocean Surface. For instance, it could happen that a persistent off-Nadir target is forcing the Tracker to follow its signal along a certain number of records. In this situation, if the ocean track section is short, the fitting result could be not representative of the ocean surface at least in the records where the off-Nadir target has an impact.

An alternative has been taken to account for solving this potential problem: to follow the geoid instead of the smoothed Window delay series. This alternative has been tested, and some results can be observed in Figure 5-3.

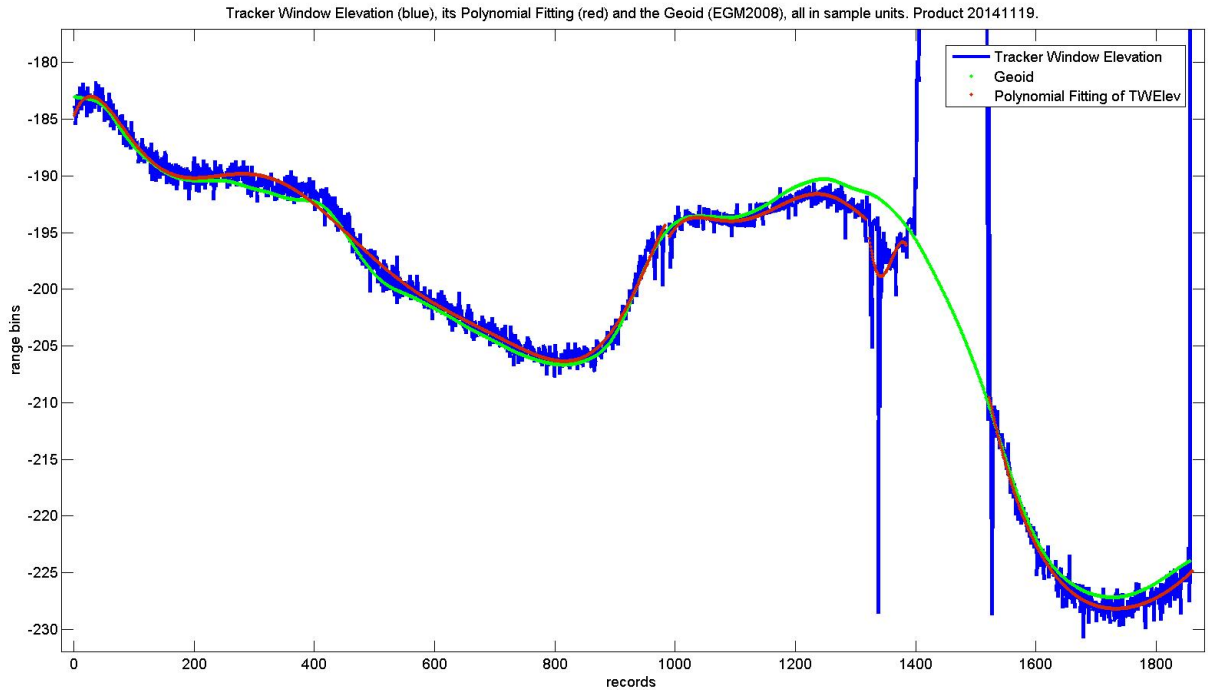


Figure 5-3. Comparison between the results of polynomial fitting (red) and the geoid (green).

We can think about the geoid as a good alternative if the Window Delay polynomial fitting fails but, at least in the Figure 5-3 case, in some intervals the geoid is not following correctly the Ocean tracking, specially when approaching the Cuban big island from the South. We could have lost the ocean signal in the south coast of Cuba if we had taken the “geoid approach” when cutting the Coastal Ocean waveforms of product of date 2014/11/19.

Anyhow, the geoid could be taken into account as an alternative for products presenting a noisy Window Delay that impacts the CP4O SSH outputs.

If we plot the Power waveforms as they come in the L1b products, we will clearly see the Window delay jumps and visually detect where the Ocean surface is located in those records. This is depicted in Figure 5-4. There we observe the link between the Window Delay jumps in the blue line of the superimposed plot and the displacements in the range direction of the Coastal Ocean power waveforms. The effect of the Window Delay corrections is the same as if we displace back in range the power waveforms the same number of waveforms they are away from the smoothed Window Delay reference.

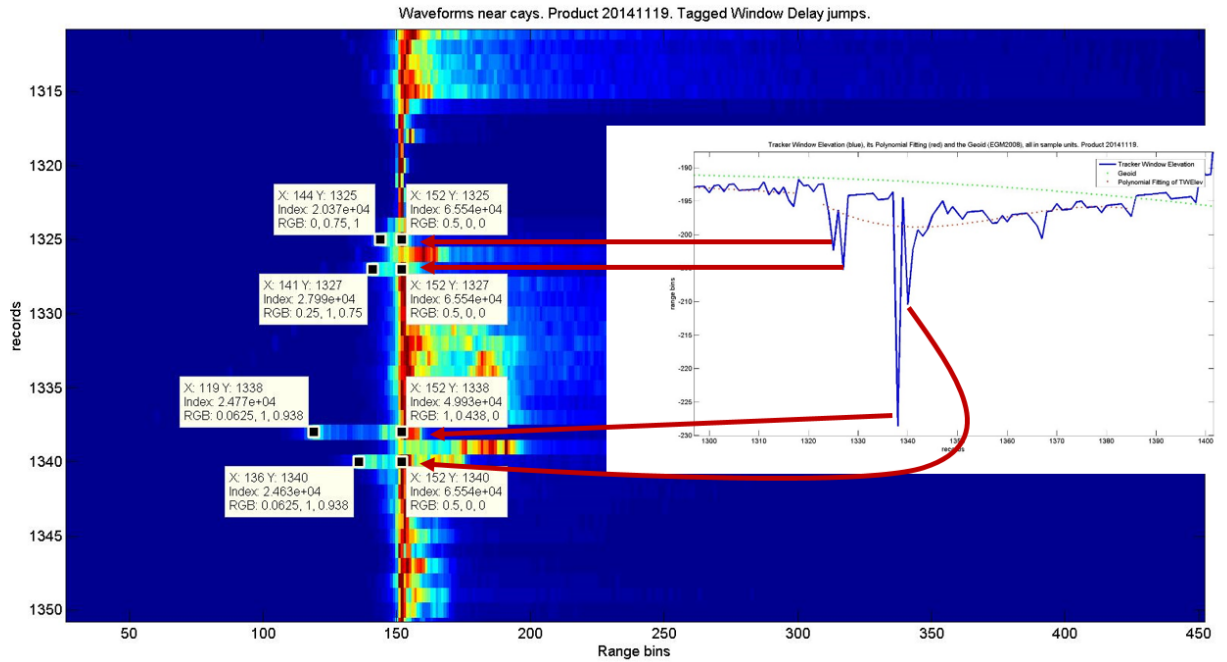


Figure 5-4. Window Delay plot (blue line) and the smoothing (red line) and geoid (green) solutions, superimposed in a Power Waveforms plot. Identification of the 4 most prominent Window Delay jumps in this track section of product of date 2014/11/19.

The ESA L2 output and the results of the proposed solution are showed in Figure 5-5 and Figure 5-6 respectively. The OSM mask has been used for filtering out the land areas.

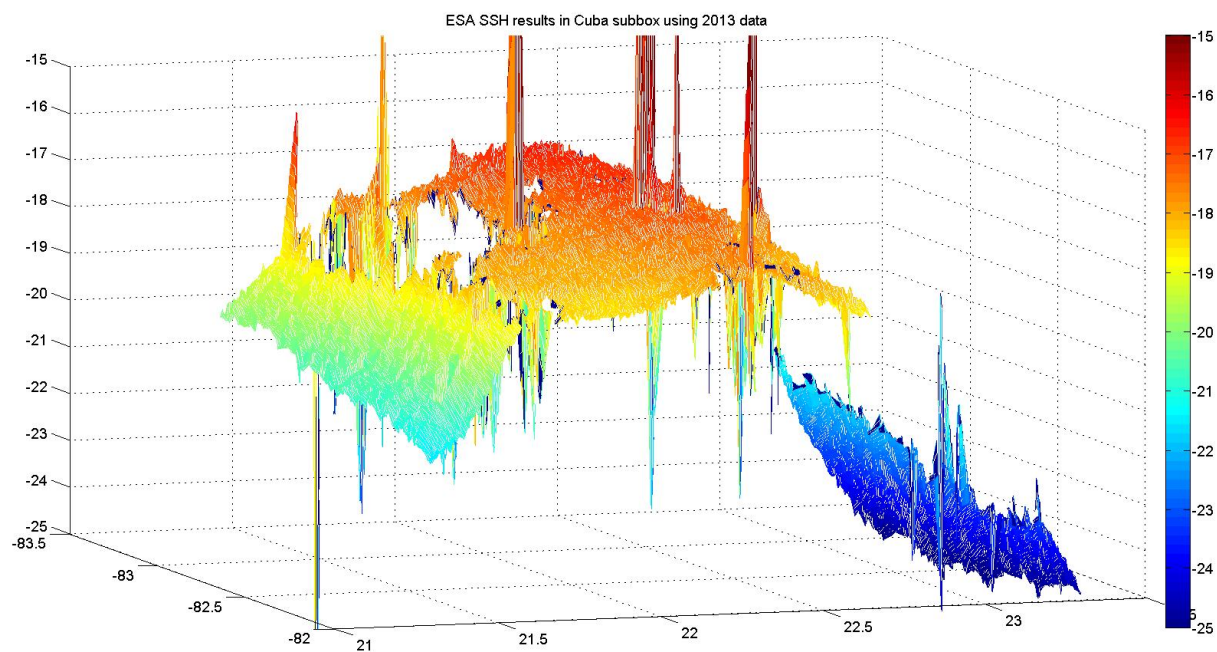


Figure 5-5. Mesh showing the ESA L2 products SSH results in 2013, masking out the land areas.
Latitude in X-axis, Longitude in Y-axis, SSH in Z-axis.

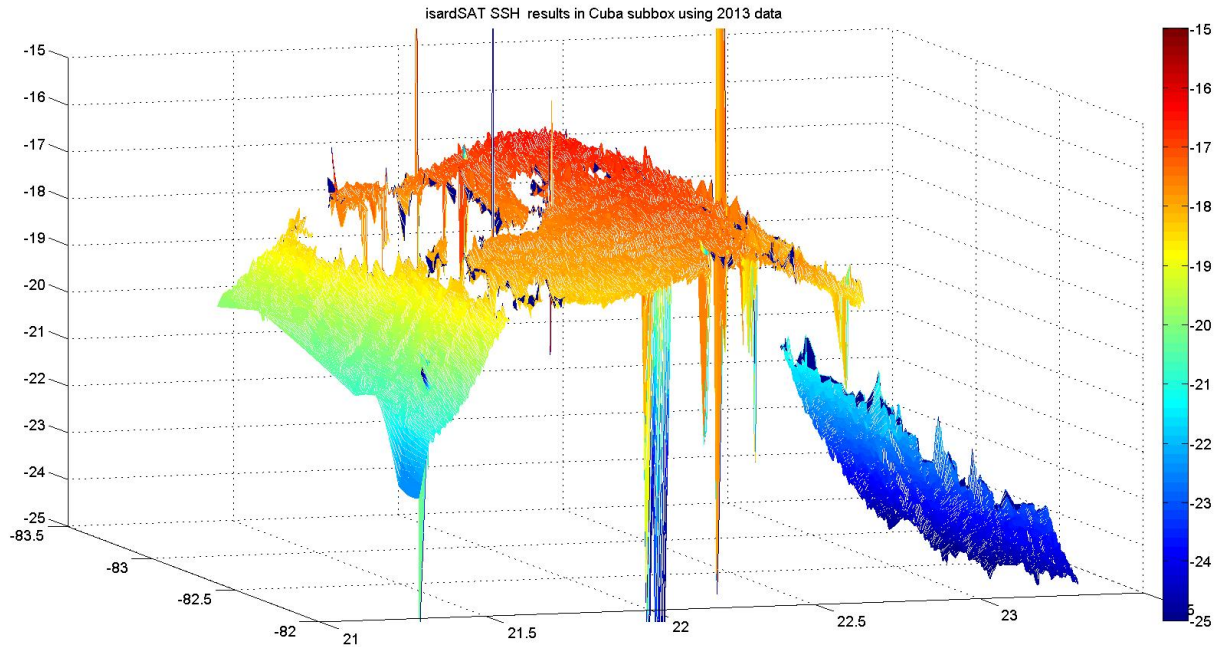


Figure 5-6. Mesh showing the CP40 SSH results in 2013, masking out the land areas. Latitude in X-axis, Longitude in Y-axis, SSH in Z-axis.

The improvement here in the coastal zones is visually evident. But there are still some spikes in the CP40 results. Nevertheless these spikes are more concentrated in areas far from the coast.

The track corresponding to the lowest SSH value (spike in the central part of Figure 5-6) has been analysed for the sake of understanding the reason of such wrong SSH estimations.

In Figure 5-7 we can see that specific track, from a product with date 2013/08/23. The records with wrong SSH estimations are circled in red, being 14 Km offshore. There is no possibility of land or coastal signals contamination. It is also specified in the figure the reach of the coastal processing, up to 5 Km offshore.



Figure 5-7. Sub-satellite track of product on date 2013/08/23. Records impacted by wrong SSH retrievals in CP40 processing are far from the coastline.

In Figure 5-8 we observe the same map, but with the power waveforms superimposed matching the same latitudes. The little island at the right part causes specular echoes, and the zone of interest for us (central records) is showing a peculiar power drop down, possibly due to a rain event in this particular area.

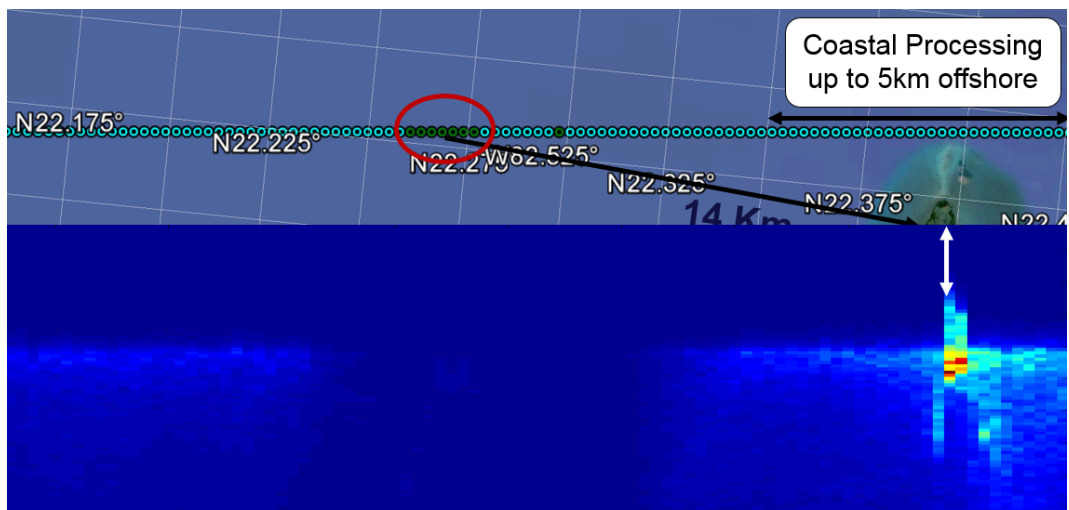


Figure 5-8. Power waveforms superimposed to Figure 5-7 image.

If we rescale the power in the zone of interest, we obtain the image of Figure 5-9. The power distribution within the echo is not the typical corresponding to an Open Ocean waveform. This is the

reason of the degradation of the SSH CP40 results. The coastal processing is not applied in these records, being farther than 5 Km from the coast.

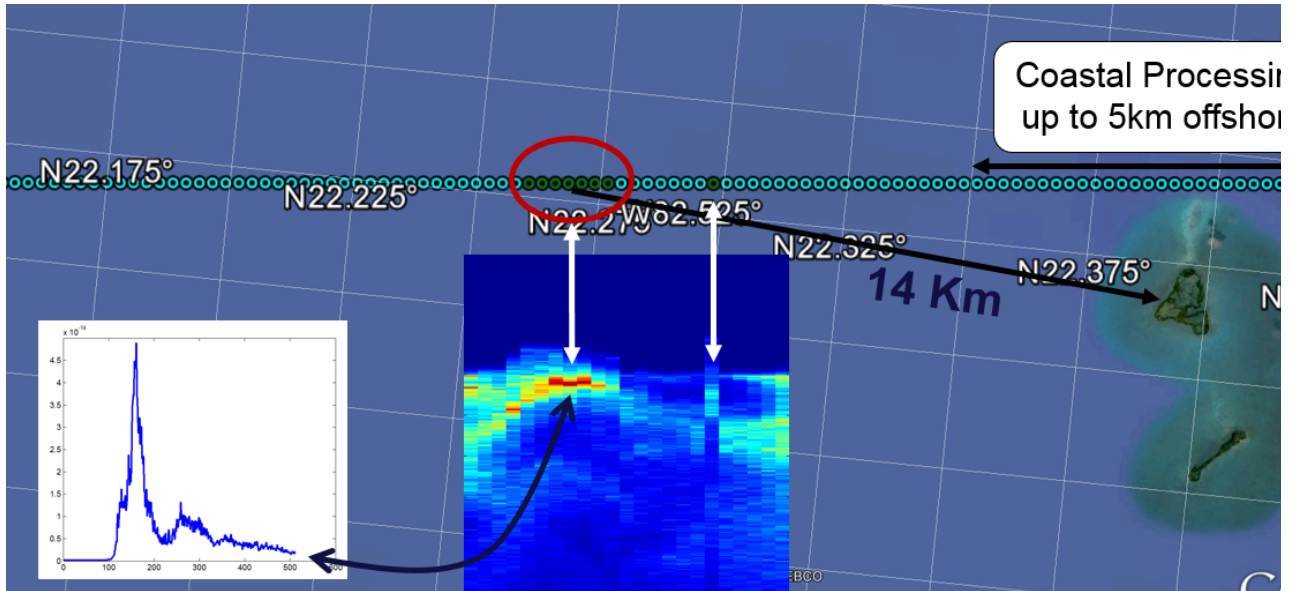


Figure 5-9. Power rescaling of central power waveforms of Figure 5-8. An example of waveform in the central records is depicted (bottom left).

The focus of this study is the coastal areas. Hence, it should be more adequate to plot only the SSH results corresponding to the coastal areas. In Figure 5-10 we can see a plot of ESA and CP40 results in areas between 100m and 5Km offshore.

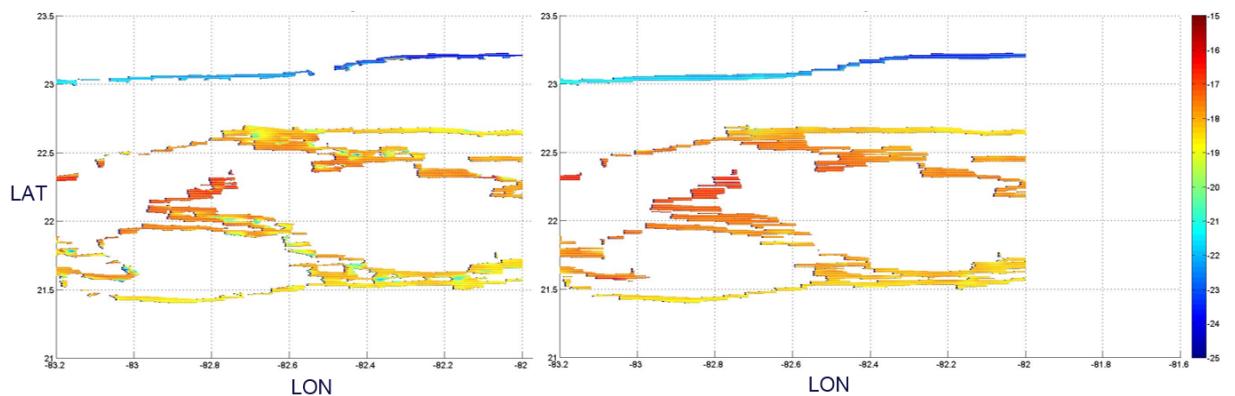


Figure 5-10. ESA (left) and CP40 (right) SSH retrievals after masking the coastal zones with the OSM mask (100m to 5 Km offshore).

The correspondent mesh figures are depicted in Figure 5-11 (ESA L2 SSH) and in Figure 5-12 (CP40 SSH).

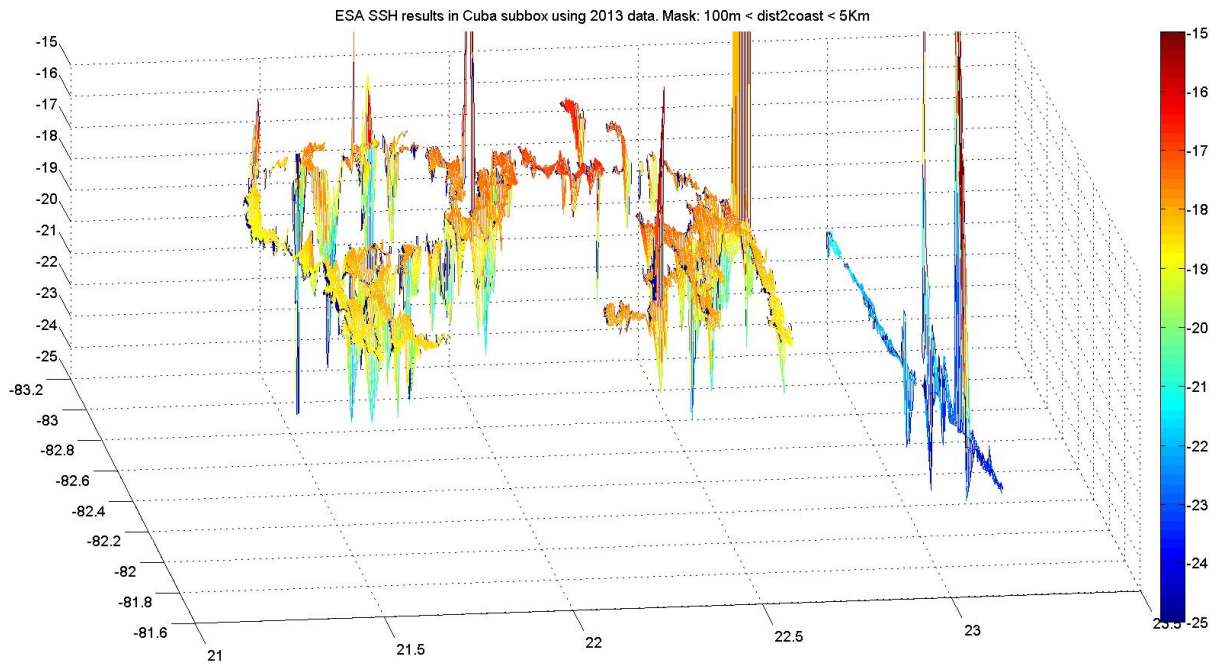


Figure 5-11. Mesh showing the ESA L2 products SSH results in 2013, masking the coastal areas. Latitude in X-axis, Longitude in Y-axis, SSH in Z-axis.

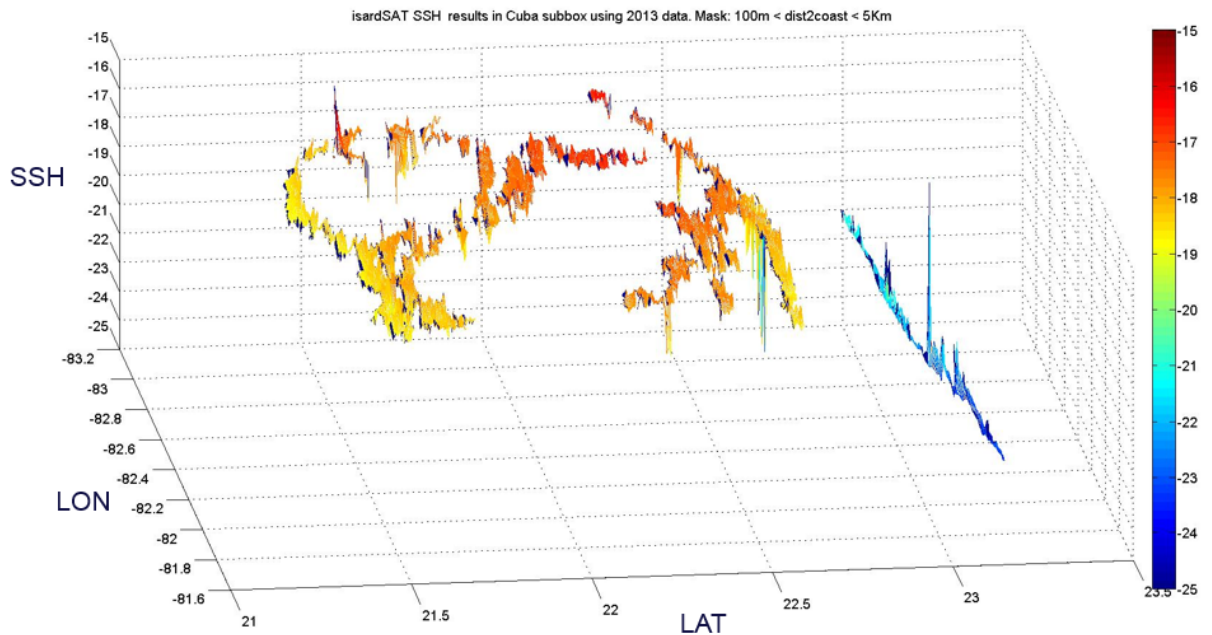


Figure 5-12 Mesh showing the CP40 SSH results in 2013, masking the coastal areas. Latitude in X-axis, Longitude in Y-axis, SSH in Z-axis.

Now the improvement becomes very evident. Almost all the ESA SSH coastal spikes are avoided. The CP40 sea surface profile is much better readable.

For showing the latitude Sea Surface profile, we can take a look at Figure 5-13. There are still some CP40 spikes in restricted coastal areas, but the overall improvement is consistent in almost the whole Aol.

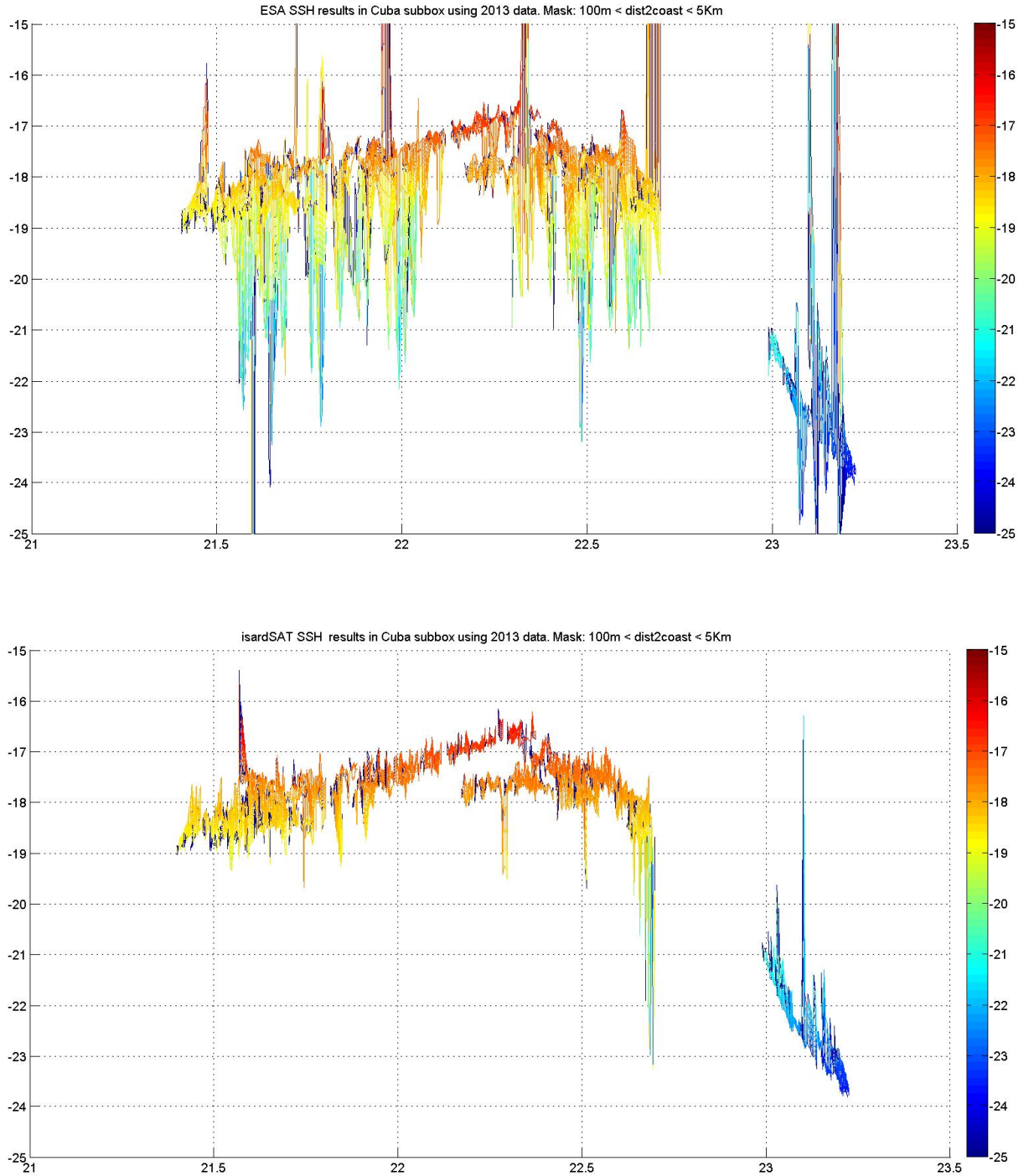
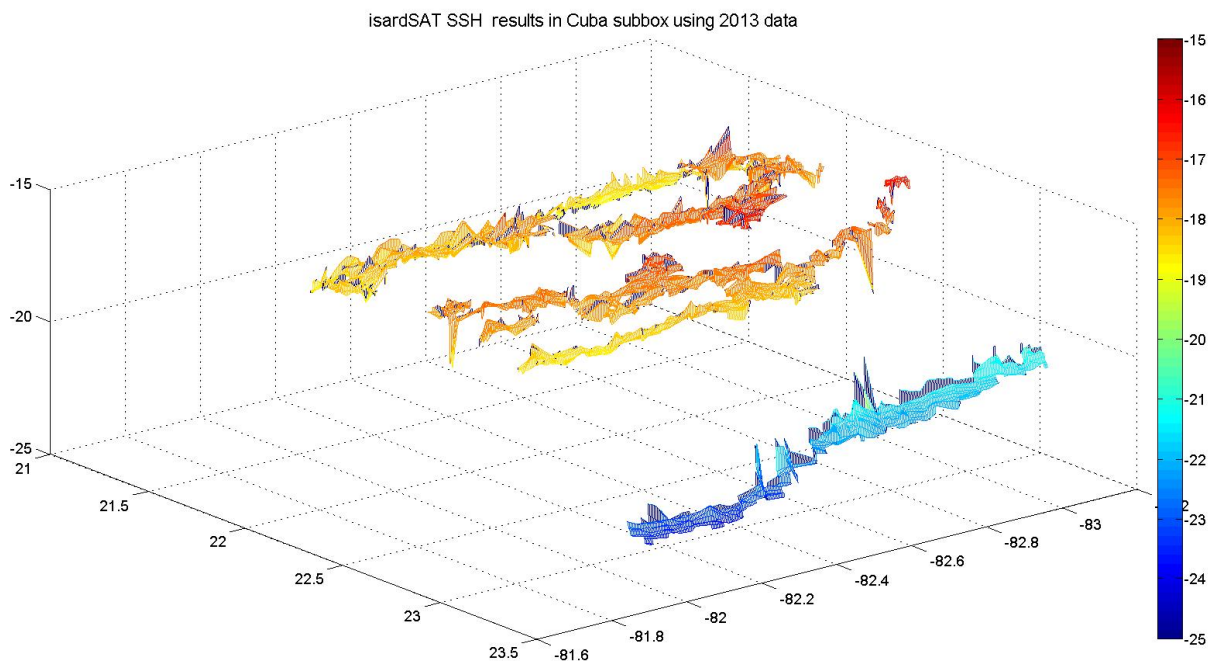
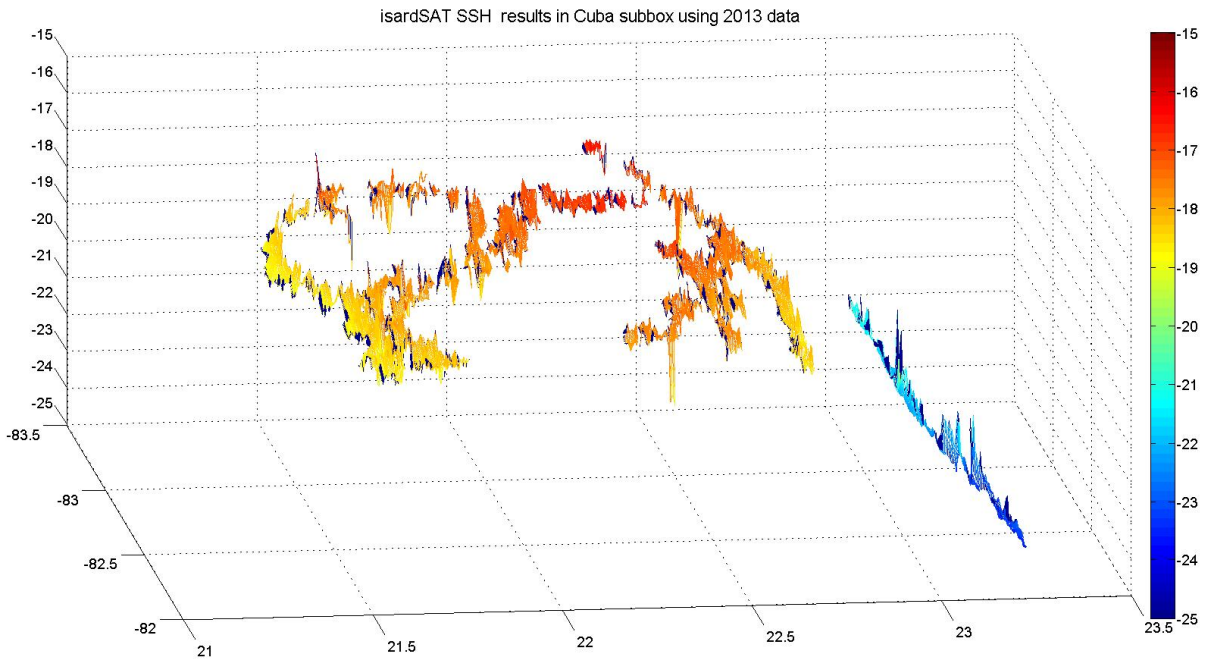


Figure 5-13. SSH profile versus latitude of ESA L2 (top) and CP40 (bottom) solutions.

5.2 Delivered Data

If we combine the geoid and Window delay approaches in three of the products with the worst coastal SSH retrievals in specific restricted areas, we obtain the results depicted in Figure 5-14.



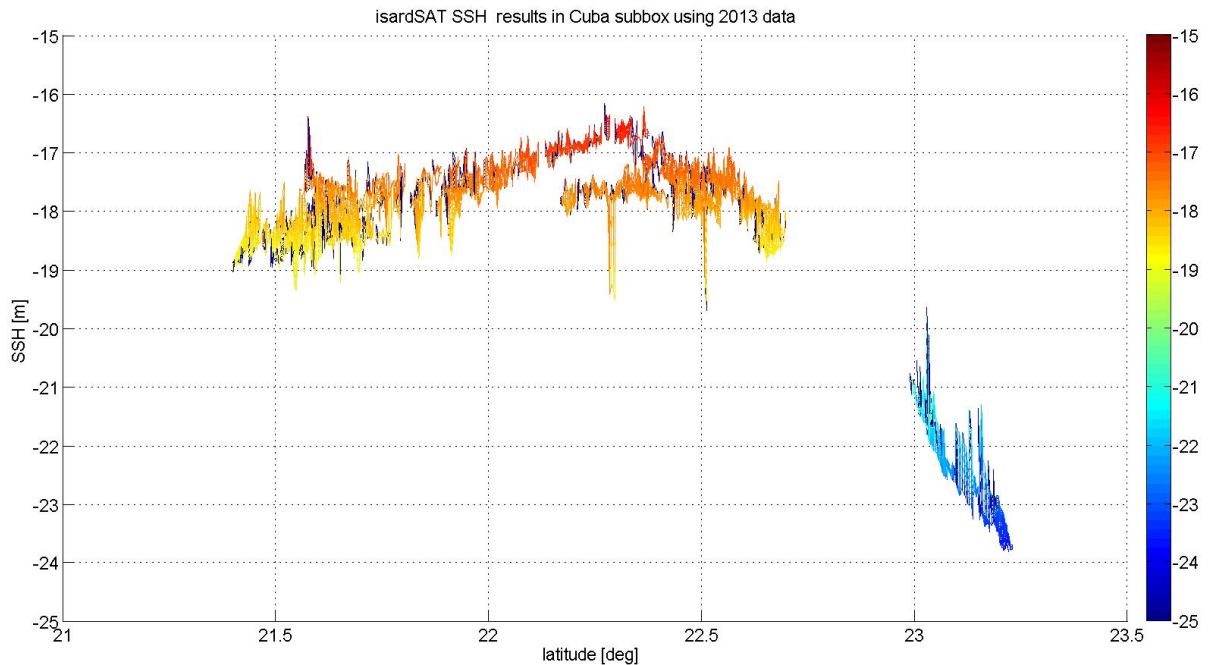


Figure 5-14. Different perspectives of a 3D plot showing the CP40 SSH retrievals after combining the Window delay and geoid approaches for the three tracks with the worst CP40 SSH outputs. Top figure: Latitude in X-axis, Longitude in Y-axis, SSH in Z-axis. Mid figure: Longitude in X-axis, Latitude in Y-axis, SSH in Z-axis.

This figure shows the final data delivered to ESA as a complete 2013 dataset. It includes the whole area data (not only the Coastal Scenario). The data is from the whole collection of 2013 year CS2 products, containing 45 tracks over the AoI.

The data is delivered as Matlab files, with two main structured variables data, the one corresponding to ESA L2 products, and the one containing the CP40 results. The variables conforming the two structures delivered are detailed here below:

- ESA data structure:
 - lat → L2 latitude (re-geolocated by the across-track distance)
 - lon → L2 longitude (re-geolocated by the across-track distance)
 - time → seconds from 2000
 - ssh → L2 ESA results
 - L1lat → sub-satellite track latitude
 - L1lon → sub-satellite track longitude
 - mask_OSM → Open Street Map mask (Km from the coast, negative if inland)
 - mask → CS2 products land-sea mask

- CP40 data structure:

- lat → sub-satellite track latitude
- lon → sub-satellite track longitude
- time → seconds from 2000
- ssh → CP4O results
- mask_OSM → Open Street Map mask (Km from the coast, negative if inland)
- ssh2plot → CP4O results masked to be plotted: from 100m to 5Km offshore.

Now, here below we provide metrics from a numerical comparison between the SSH estimates of the above mentioned ESA and CP4O datasets.

First, a standard deviation has been computed at different scales. A raw comparison of the 20 Hz SSH standard deviation for the whole dataset is shown in Table 5-1.

Comparison of overall SSH standard deviation	
ESA dataset	CP4O dataset
2.6985	1.5671

Table 5-1. Standard Deviation of ESA & CP4O datasets

But the above crude result incorporates the big jumps of SSH between products, and also between each individual coastal ocean track section. Hence, a more realistic approach is to show the standard deviation of each track section 20Hz SSH (see Figure 5-15). More than 300 sections were detected in the complete dataset.

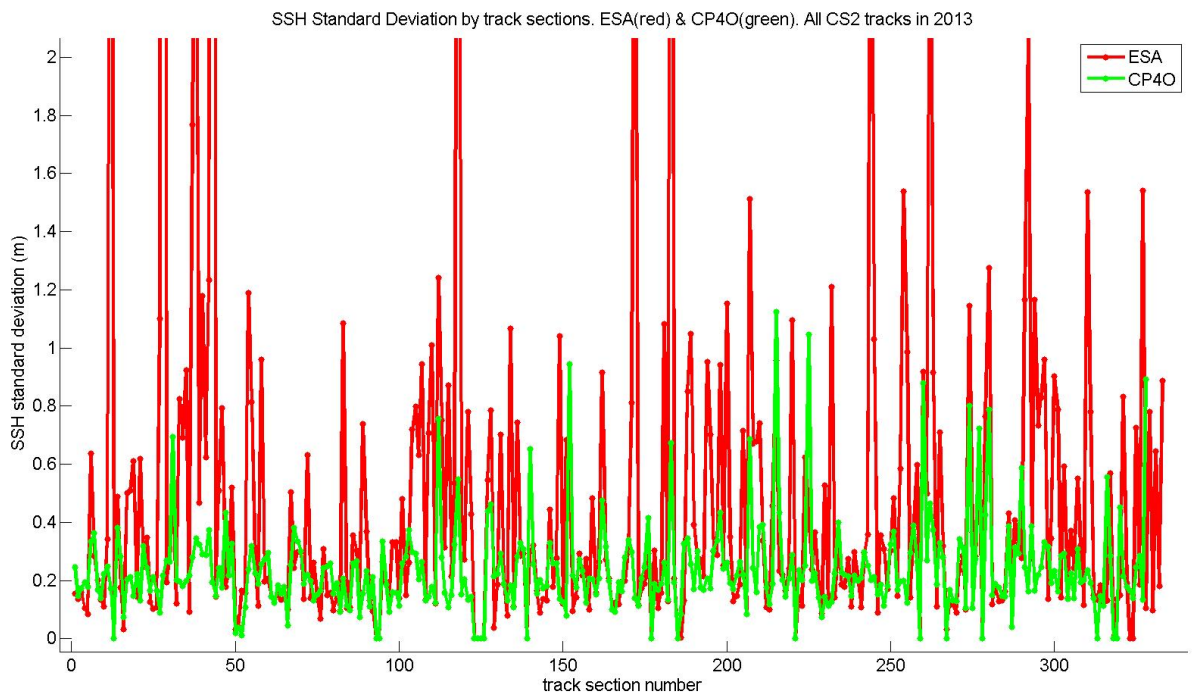
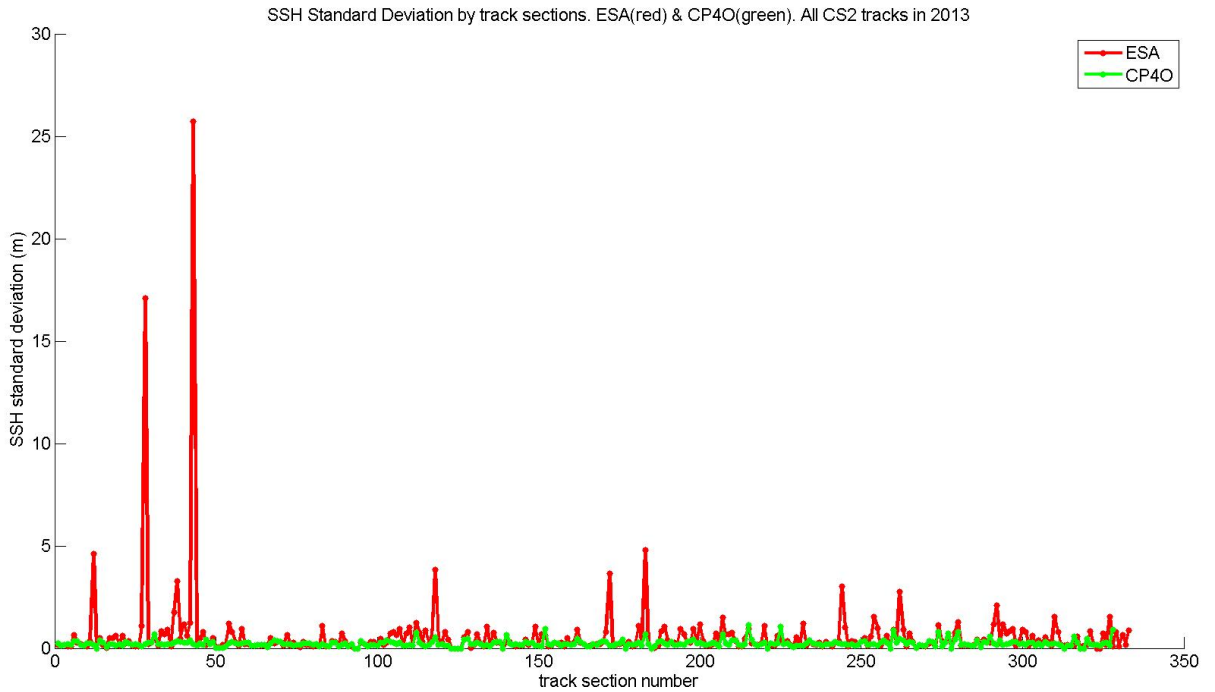


Figure 5-15. 20 Hz SSH standard deviation of ESA (red) & CP40 (green) by coastal ocean track sections. Bottom figure shows a zoom of Top figure around CP40 values

The above figure statistic results show the real standard deviation of the data corresponding to each of the track sections. With this approach we do not mix the along track SSH stability with the SSH jumps between track sections. The above plot Figure 5-15 is translated into averaged numerical results in Table 5-2.

Averaged SSH stdev by track section	
ESA dataset	CP4O dataset
0.5819	0.2345

Table 5-2. Results of an averaging of the SSH standard deviation by track sections for the ESA and CP4O datasets.

From the results showed in Table 5-2, we can see that the improvement of the SSH standard deviation in the whole area, measured by track sections, is about **60%**.

This is a remarkable outcome of the current study.

On the other hand, if we look at the performances of the SSH retrievals considering the distance to the closest coast point, we could have a perception of how the two SSH results behave while approaching our area of interest from the Open Ocean.

The results of the 20 Hz SSH series versus the distance to the coast can be observed in Figure 5-16. It has been done for a distance of 100m to 5 Km offshore, the same used for the 3D plots of previous sections. We can detect in Figure 5-16 (Top figure) a number of ESA SSH outliers along the whole section.

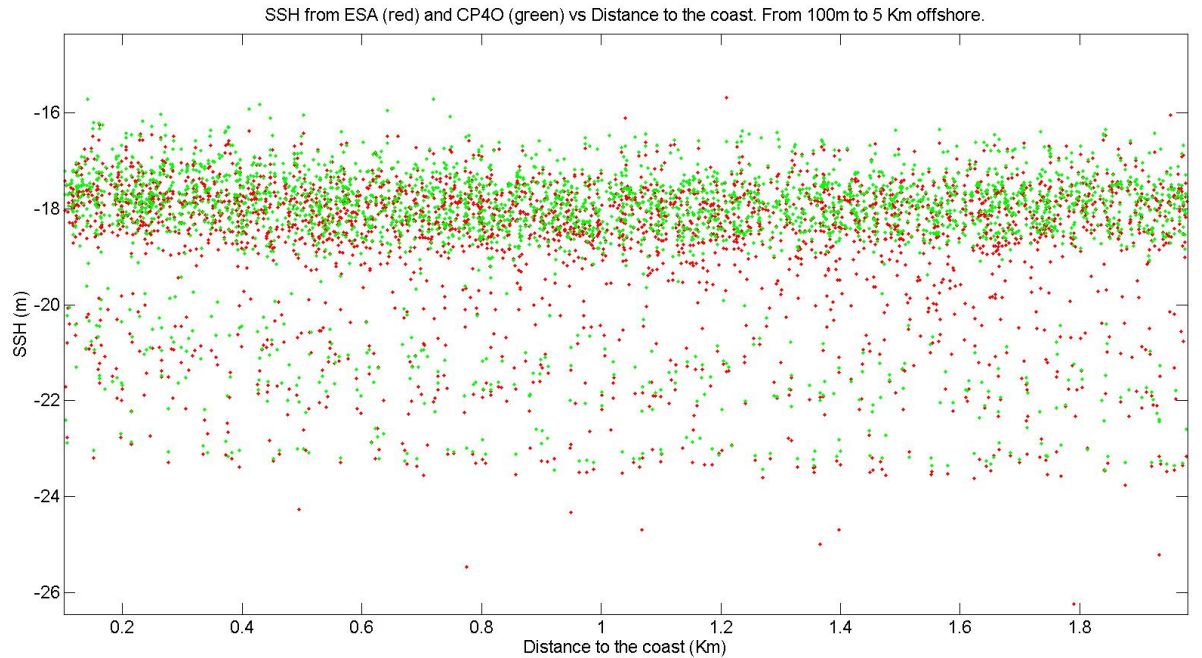
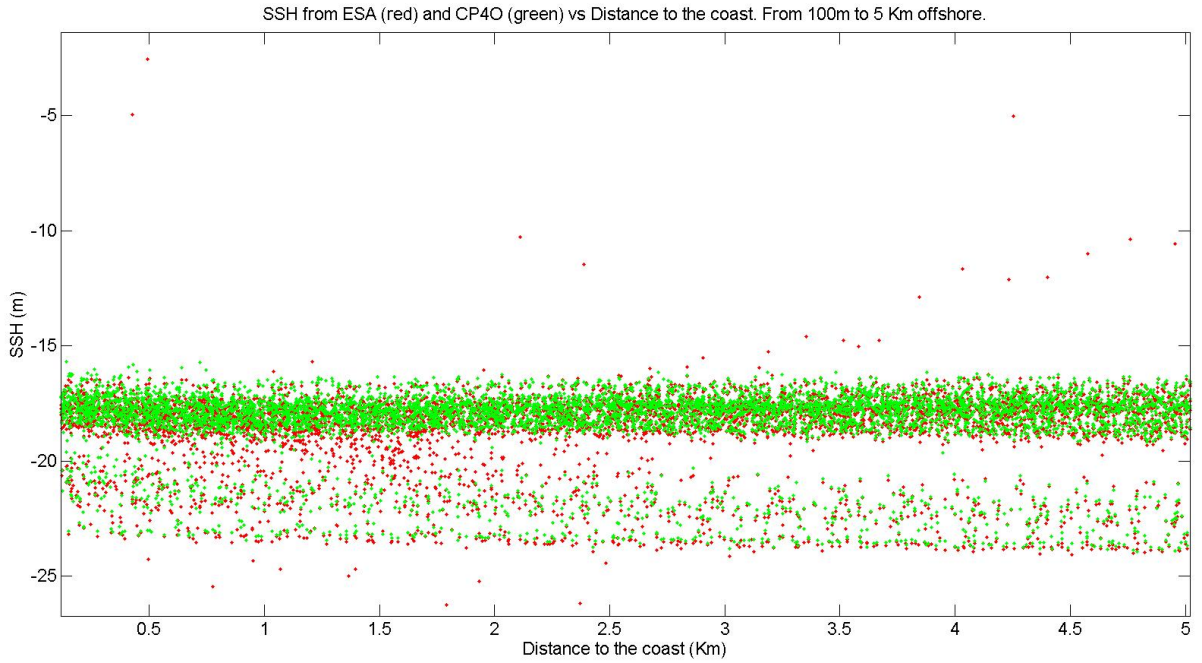


Figure 5-16. 20 Hz SSH differences along the track versus distance to the coast. ESA in red, CP40 in green. Bottom figure shows a zoom of Top figure around CP40 values.

For a better understanding of the SSH stability, the difference between 20Hz records along every track has been analysed, and been plotted against the distance to the coast. The output of this

computation is depicted in Figure 5-17. The less stable the series, the higher results ($\text{abs}(\text{diff}(\text{SSH}))$) we will see in the figure. We can clearly see that the stability of SSH reduces as the coast is approached for both series (ESA & CP4O), and the improvements in the CP4O data for the AoI along the whole studied set of data, from 100 meters to 5 Kilometres offshore.

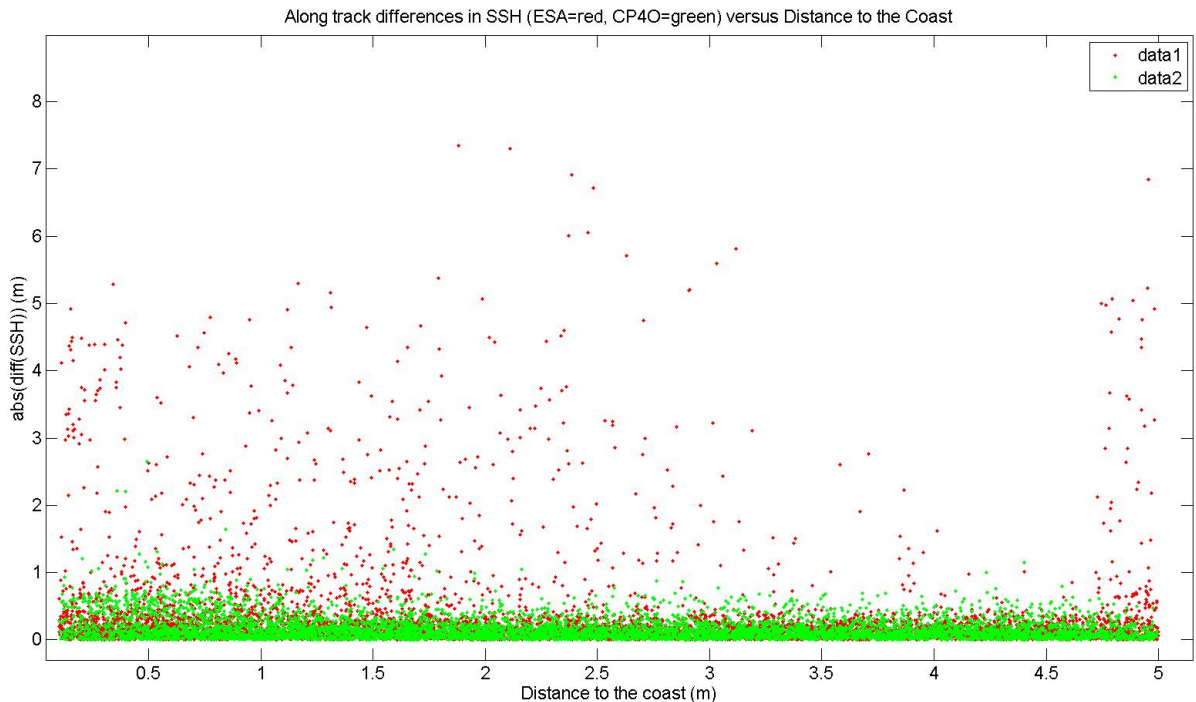


Figure 5-17. SSH differences along track versus distance to the coast. ESA in red, CP4O in green.

Finally, two more computations were done to provide the best understanding of the 20 Hz SSH stability performance for the ESA and CP4O datasets. The same data plotted in Figure 5-17 has been averaged into sections of distance to the coast, every 100 m and every 10 m. This is shown in Figure 5-18 and Figure 5-19 respectively.

From Figure 5-18 (averaged every 100 m offshore), we see a clear detachment of the ESA results with respect to the CP4O results from around 3500 m offshore to distances closer to the coast. In that offshore distance range, the CP4O shows a neat better stability. The CP4O data shows a worsening of the 20 Hz SSH standard deviation from around a constant 14 cm from 2 Km offshore, to around 30 cm when about few hundreds of meters from the coast. A standard deviation of 20 cm is achieved around 800 m offshore for CP4O results. Furthermore, if we take the best ESA results along the whole offshore distances span, its SSH standard deviation goes from results similar to CP4O from 3500 m offshore (around 14 cm), to more than 30 cm at 2000 m offshore, and finally around 60 cm close to the coast. The improvement in the CP4O results is evident.

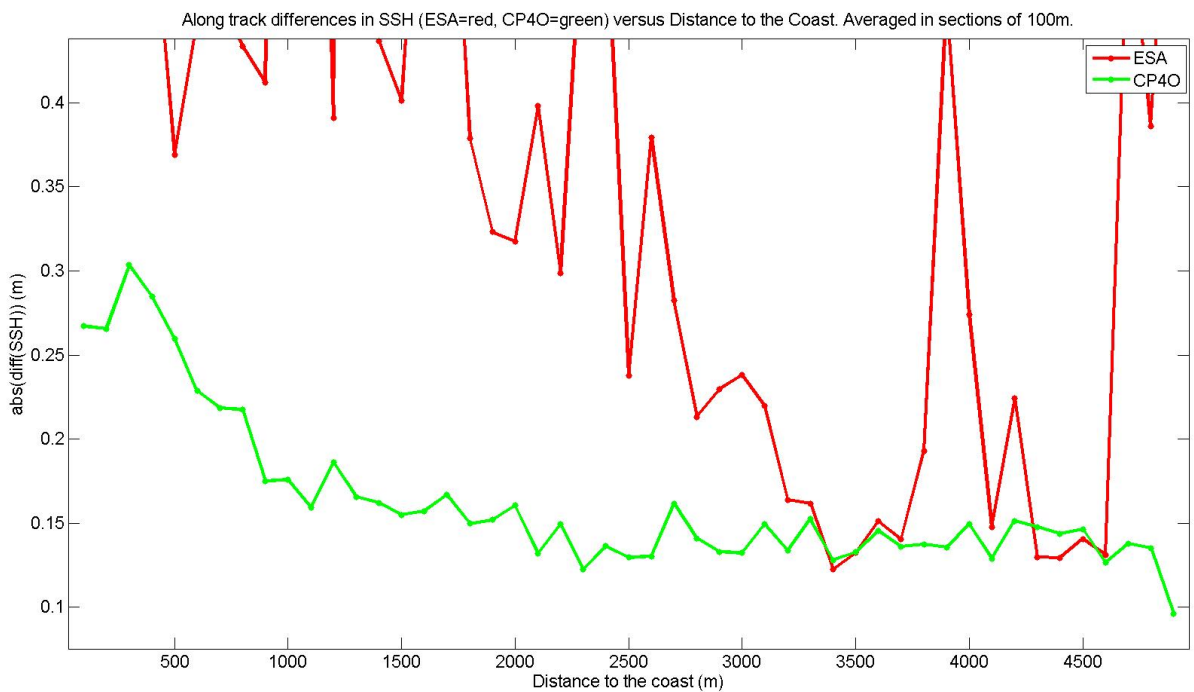
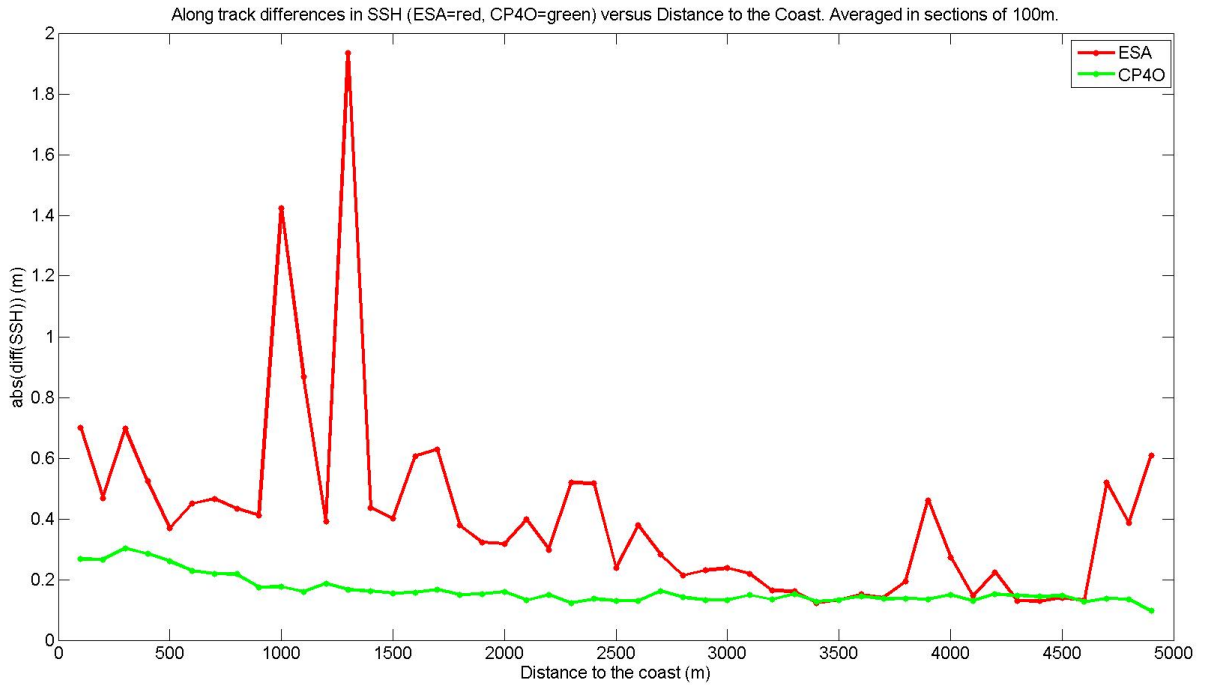


Figure 5-18. SSH differences along the track versus distance to the coast, averaged every 100m. ESA in red, CP40 in green. Bottom figure shows a zoom of Top figure around CP40 values.

A final figure (Figure 5-19.) illustrates a finer resolution in the results by averaging offshore distance every 10 meters. The same outcome can be observed: a better performance of CP4O 20 Hz SSH stability if compared to ESA results. In this new figure we can also observe how the variability of the standard deviation is higher for ESA than for CP4O, this last showing only one clear outlier over 40 cm in the whole dataset of 10m sections of distance to the coast.

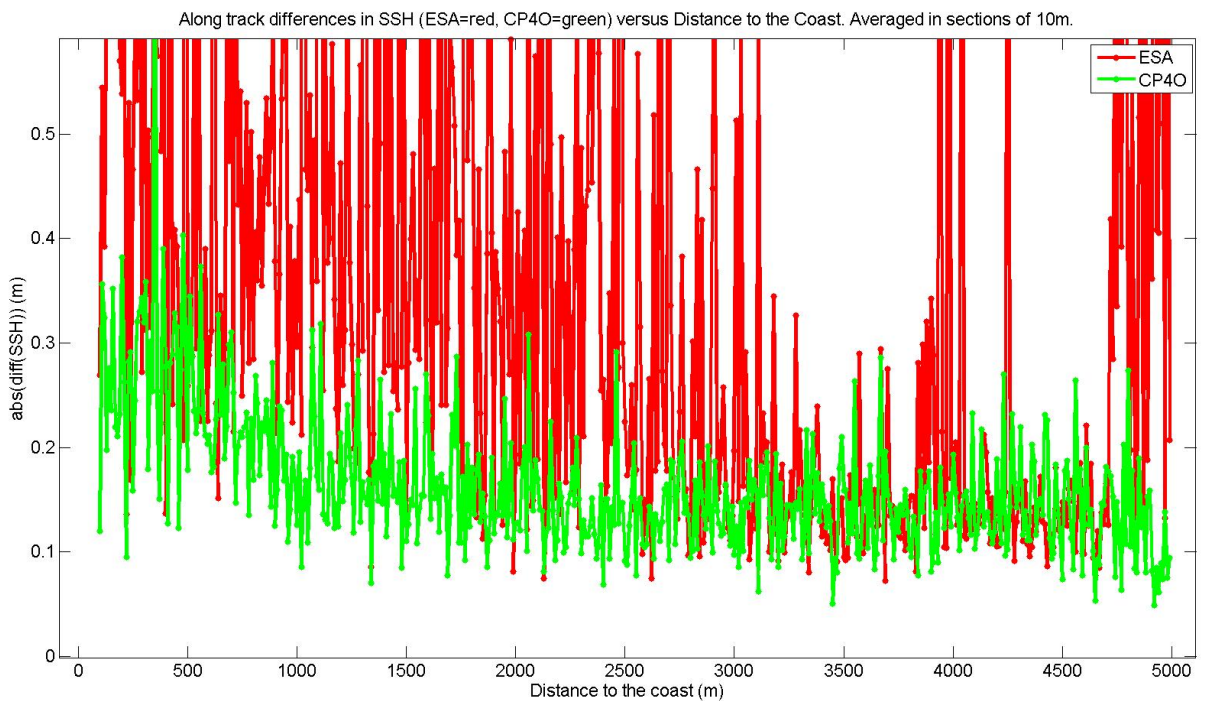
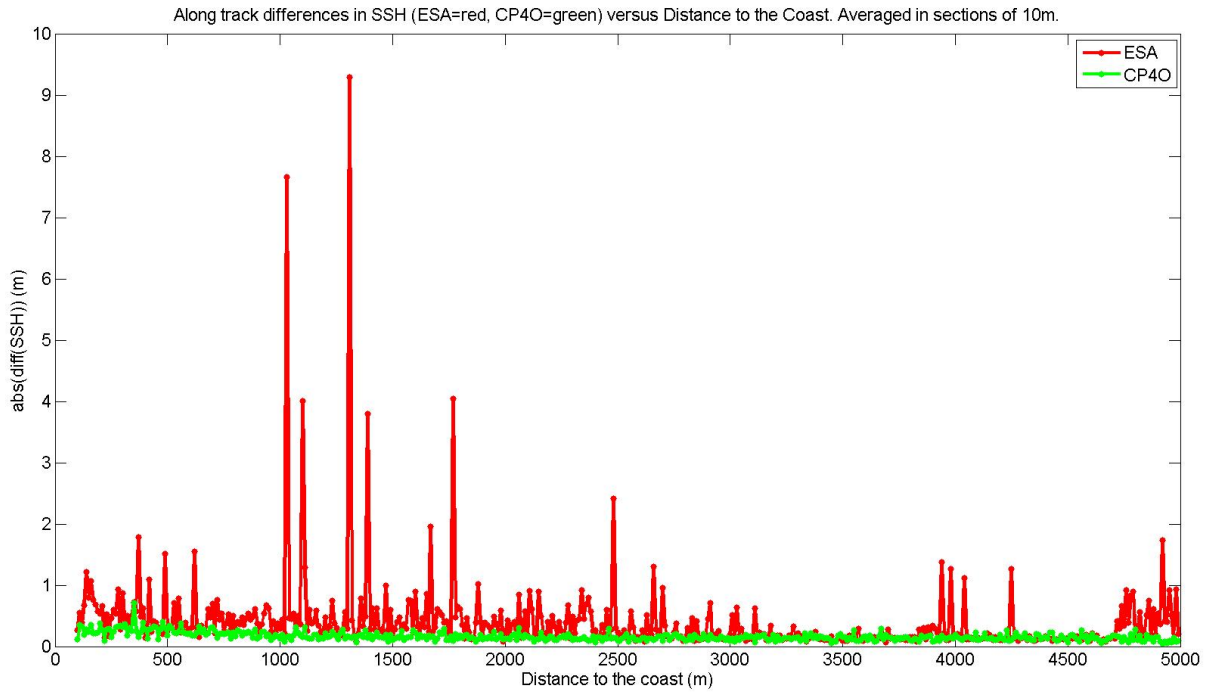


Figure 5-19. SSH differences along the track versus distance to the coast, averaged every 10m. ESA in red, CP40 in green. Bottom figure shows a zoom of Top figure around CP40 values.

5.3 Open Ocean retracker assessment

The results from the retracker explained so far are corresponding to the coastal processing developed within this product. But the SSH retrievals are also produced for echoes far from the coast (more than 5Km offshore).

In this subchapter we explain a little assessment on the SARin retracker developed by isardSAT (inherited from the SAMOSA retracker) in an Open Ocean scenario.

For this purpose we focused the assessment in a track inside the AoI (see 3.2) with a long track section farther than 5 Km from any coastline. The track selected is the one of date 2013/05/02, with a long track between Isla de Pinos and Cuba.

The track section goes between latitudes 21.8 N and 22.2 N, as showed in Figure 5-20. Its length is about 45 Km.

For the assessment, a running window was computed summing the residuals from a quadratic polynomial fitting of the SSH series (output of the retracker) over each window position on the track section. The window width used was 20 records. A sum of the above values along the track gives us an idea of the retracker performance over Open Ocean.

The assessment result shows us that the CP40 retracker over Open Ocean is notably improving the ESA L2 retracking outputs, as specified here below.

ESA results: 12.07 cm

CP40 results: 7.51 cm

The improvement of the retracker performance is close to a 45%.

A plot of both SSH series is depicted in Figure 5-21. It is clear that the SSH retrievals of the CP40 retracker option along the Open Ocean track section have a higher stability. Again, we want to clarify that the coastal retracking is not applied here. In Open Ocean the SARin retracker process the whole science waveform instead a cut section of it as is done for the coastal scenarios.

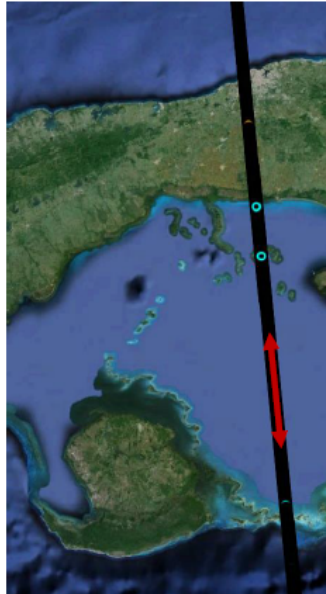


Figure 5-20. Track selected for an assessment of the retracker results over Open Ocean. In red is highlighted the track section analysed.

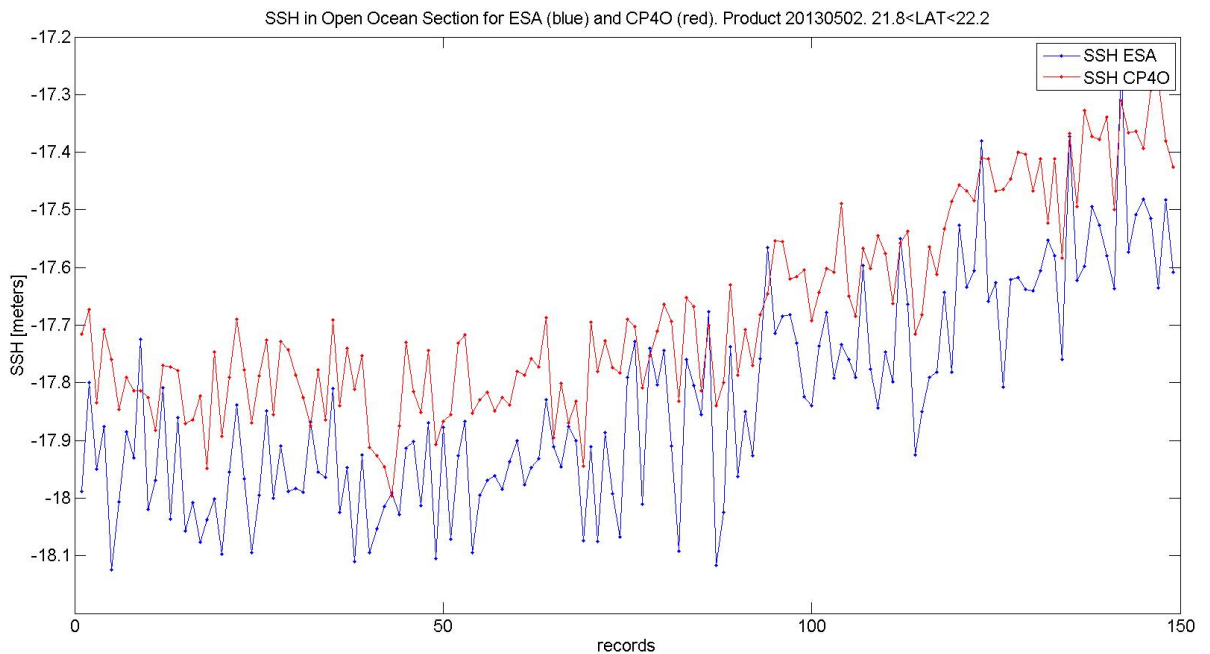


Figure 5-21. SSH series over Open Ocean. ESA in blue, CP40 in red.

6 Conclusions

The SARin for coastal processing developed in the first phase of the CP40 project has been updated in the second phase to new algorithms that improve the former SSH results. The processing in the first phase consisted in a post-L1b stage that produced a seed used as a reference for a retracking (second stage) processing.

As AoI, it was considered a sub-box (see 3.2) inside the Cuba SARin mode geographical mask, presenting different cases of coastal topography scenarios, with several coastlines geometries, etc.

A first option (see 4.1) was implemented interpolating the undesired (away from Nadir) range bins in the science SARin waveforms. The results were better than in the first phase, especially when the contamination was located in range bins far from the leading edge point, and those targets were not spread all over the waveform. The retracker processed the whole transformed science waveform.

In several cases where the above conditions were not fulfilled the results were not satisfactory. Then, a second option (see 4.2) was developed, where the SARin waveform is cut around the closest to Nadir range bin (i.e. the seed). In this case, the retracker processed a cut waveform, from the thermal noise level last sample before the ocean surface signal to ten samples after the seed.

With this second option the results were improved with respect to the first one. But in some cases the SSH retrievals were not good due to a degradation of the mean variable to retrieve the seed: the Phase Difference SARin variable.

It was not expected that in some coastal zones, the ocean signals did not show any range bin close to Nadir (all the phase difference values inferred across-track distances of more than 500 meters) in a series of consecutive records in the track. Then, the seed was not able to be derived, and so we had no reference to cut the waveform for the retracking processing.

A third option (see 5.1) was developed to overcome the above problem, with the constraint of not using the Phase Difference data. The problem was turned into an advantage.

The new variable identified for producing the seed for the retracker was the Window Delay. It was supposed that the on-board tracker jumps near the coasts were due to the presence of contamination in the echoes, that lead the tracker to follow the contamination targets instead of continuing the Ocean signal tracking. If we knew the Window Delay jump amount, we could correct it and give the retracker the correct waveform cut section to retrack, and therefore clean the waveform from the contamination signals. For the implementation of this option, a polynomial fitting (dynamic degree) was done to the Window Delay series in every ocean section of the track, and the residuals of the fitting were used for the seed production.

For the ocean sections determination it was implemented a land sea mask from the OSM. The GSHHS and Coastal Proximity Parameter (Paolo Cipollini, NOC) masks were also considered but with not satisfactory results due to the level of coastal topography complexity in the AoI selected.

This third approach has a huge advantage: it is useful not only for CS2 SARin data, but also for the other CS2 two modes: SAR and LRM. And also for other altimetry missions like EnviSat and Jason1/2 (LRM) or S3 and S6 (SAR). The processing shall be adapted in such cases (e.g. the retracker processing stage shall be modified).

The results of the third approach substantially improve the coastal zones (100m to 5000m) SSH retrievals. Figure 5-13 is the visual evidence of it, showing the coastal zones SSH retrievals for ESA L2 and CP4O in 2013.

An alternative to the use of the smoothed Window Delay could be to use the geoid (EGM2008), but it was detected in some cases that the geoid model was not following properly the tracker window stabilised behaviour, and therefore it was not a good option to follow the Ocean signal. In any case, the geoid option could be an alternative in case the Window Delay option fails, as it happens when the tracker follows a coastal (non Nadir ocean) target in a continued series of records.

A database is delivered (see 5.2) considering the year 2013. Both ESA and CP4O SSH series are in the database for comparison, including coastal and non coastal processing. The third option was considered for the deliverable, and some few records of 3 of the 45 products showing wrong SSH estimates were substituted by the geoid option. Figure 5-14 is representing the CP4O output delivered.

To provide a numerical assessment of the improvements in 20 Hz SSH measurements resulting from this study, the standard deviation of each individual section of the dataset (a total of more than 300 sections) were computed. The benefits of the approach developed in this study were clearly seen in the averages of standard deviations of all the sections. The average SSH standard deviation from the new CP4O scheme was 60% lower than that calculated from the ESA products (see Figure 5-15 and Table 5-2). The improvement is even greater if data closer to the coast are considered

Also the SSH along track differences versus distance to the coast were presented for both ESA & CP4O series, in order to study the stability in the SSH data while approaching the coast (see Figure 5-17, Figure 5-18 & Figure 5-19). Here again, the results from the new approach demonstrated a more stable behaviour than seen in the ESA results. The CP4O and ESA series presented similar SSH along track differences, around 14 cm, when far from the coast (more than 3500 meters), but when approaching the coast a clear difference in behaviour was seen with CP4O SSH along track differences of up to 30 cm and ESA SSH along track differences of more than 60 cm for a distance offshore of few hundreds of meters. Again, an improvement of over 50% has been observed.

Finally, an assessment (see 5.3) was done to check the CP4O retracker performance over Open Ocean. The improvement with respect to the ESA L2 retracker SSH results was up to 45%.

An interesting application of this implemented coastal processing could be to develop a MSS database of this specific area by processing a data series over a period of several years. Of course, the Aol could potentially be any other around the world, and the data could also come from other CS2 operational modes, and even from other missions; in this case the algorithms must be adapted.

In terms of future work for improving the above solution for coastal altimetry, there are some ideas that could be developed for improving the current CP4O results. The SAR mode enables the possibility of a dedicated stack processing that could lead to a less contaminated multilook waveform. The algorithms here explained could be combined with a stack processing in order to give the retracker not only a seed and a cut waveform avoiding interferences, but also work with an enhanced multilook waveform pre-processed for better further SSH retrievals. For echoes very close to the coastline, steering could be also an additional help for improving the results. These are major modifications to the current processing as they are not starting from already processed L1b SARin products, but modifying the L1b SAR/SARin processing.

in summary, we have analysed the results of two approaches:

- Firstly, one for SARin data, using the Phase Difference information to produce the retracker seed

- Secondly, an approach that can be applied to SAR and LRM data (and also SARin), using the Window Delay information for the same purpose

An interesting option for further studies is to combine the two above approaches in a synergic solution that takes the best from both, and derive an enhanced SSH coastal mapping.